



National & Kapodistrian University of Athens
Department of Physics
Section of Environmental Physics and Meteorology

Athens, March 2021

A study of the evolution of clouds during a cold air outbreak
with the use of numerical simulations



Source: <https://worldview.earthdata.nasa.gov/>

Michail Karalis

Master Thesis



National & Kapodistrian University of Athens
Department of Physics
Section of Environmental Physics and Meteorology

Athens, March 2021

A study of the evolution of clouds during a cold air outbreak
with the use of numerical simulations



Source: <https://worldview.earthdata.nasa.gov/>

Michail Karalis

Supervisory Committee:

Maria Tombrou-Tzella (main supervisor) :	Professor,	NKUA
Georgia Sotiropoulou :	Postdoctoral Researcher,	SU
Elissavet Bossioli :	Assistant Professor,	NKUA

Acknowledgements

I would like to express my deepest gratitude to my supervisor, Professor Maria Tombrou-Tzella, for her trust and support throughout the course of my studies. Her insightful remarks, encouragement and admirable work ethic were crucial for the completion of this dissertation and made my first research endeavors an unforgettable experience.

I am also grateful for the continuous help, unwavering commitment and guidance of Dr. Georgia Sotiropoulou who played an instrumental role in the orchestration of this project. In addition, I would like to sincerely thank Dr. Elissavet Bossioli for her timely suggestions and her major contribution to the continuation of this study, as well as the doctoral student Georgia Methymaki who was always available to assist and advise me during my training.

Finally, I would like to thank Dr. Steven J. Abel and Dr. Philip R. A. Brown, who generously provided us with the observational data from their experimental campaign (Abel et al., 2017). Their article constituted the main motivation of this study and helped determine the direction and premise of our research.

Contents

Abstract	5
1. Introduction	6
2. Theoretical Background	8
2.1 Cold Air Outbreak	8
2.1.1 Climatological and Meteorological features of CAOs	8
2.1.2 Planetary Boundary Layer Structure and cloud cover	10
2.1.3 Future projections for CAOs	11
2.2 Stratocumulus-to-Cumulus Transition	12
2.3 Cloud Microphysical Processes	15
3. Methodology	22
3.1 Area of study and prevailing atmospheric conditions	22
3.2 Aircraft Measurements	23
3.3 Simulations	24
3.4 Microphysics parameterizations	26
4. Results	28
5. Conclusions	38
6. References	40

Abstract

A stratocumulus-to-cumulus transition (SCT) is a change in the cloud morphology, typically observed in cold air outbreak (CAO) episodes and suggested, by recent studies, to be driven by microphysical and precipitation processes which are highly underrepresented in general circulation and climate models. Using the Weather Research Forecasting (WRF) model, a set of simulations is performed on an SCT case observed to the north of the UK on 24/11/2013 by Abel et al. (2017) in order to test the effect of secondary ice production (SIP) mechanisms on the initiation and evolution of the transition. Of the SIP mechanisms tested (collisional break-up, droplet-shattering, Hallett-Mossop), collisional break-up was found to be the most impactful in generating precipitation-sized particles and decreasing the liquid water path (LWP) in the convective region, to values comparable to measurements (Abel et al., 2017) while the results also showed a considerable dependency on the assumed rime fraction of the colliding particles. The impact of the Hallett-Mossop mechanism, despite its vast implementation in weather prediction models, appeared to be insignificant.

1. Introduction

During the past century, atmospheric scientists have unanimously concluded that clouds strongly influence our planet's climate system. Their interaction with solar and terrestrial radiation contributes greatly to the tropospheric diabatic heating which has an implicit effect on the atmospheric circulation and the planetary energy transport by the atmosphere and the oceans. In addition, the intricate microphysical cloud processes have major impact on the Earth's energy budget, due to the release and absorption of large amounts of latent heat while, the precipitation that usually accompanies the formation of clouds constitutes a key mechanism of the hydrological cycle.

Although the role of clouds in regulating the climate system has been highlighted in several studies (e.g. Chen et al., 2000, Bony et al., 2006, Taylor et al., 2012), the representation of complex cloud processes in meteorological and climate models has not yet been fully achieved. The main reason for that is that the resolvable grid scale of most mesoscale and planetary models is too coarse to successfully incorporate cloud microphysical processes. Therefore, the development of sophisticated parameterization schemes in order to reduce the uncertainty in model predictions, has become increasingly necessary.

One example of a phenomenon that is often poorly simulated in climate and general circulation models is the Stratocumulus-to-Cumulus Transition (SCT) (Soden and Vecchi, 2011, Xiao et al. 2012). Such changes in cloud morphology can usually be observed when cold air masses are advected over warmer aquatic surfaces, an event also referred to as cold air outbreak (CAO). The coupling of microphysical processes, dynamics and convection in the shallow boundary layer poses a great challenge when modeling cold air outbreaks.

A case of an SCT that occurred during a CAO, to the north of the United Kingdom, was captured by Abel et al. (2017) using aircraft observations and simulations. That study shed a new light on the mechanism of the transition, with the authors maintaining that the increasing sea surface temperature and cloud top entrainment, which were once believed to be the driving factors for the SCT, do not contribute significantly to the cloud breakup. In contrast, they claimed that the transition is mainly induced by the formation of precipitation which, in turn, is largely controlled by the Hallett-Mossop mechanism (1974).

Abel et al.'s findings provided major inspiration for this particular study. Following the direction indicated by their research, we use the Weather Research and

Forecasting (WRF) mesoscale numerical model to focus on the role of cloud microphysics by enlisting more sophisticated parameterizations of Secondary Ice Production Processes (SIP) in order to assess their impact on the transition. The purpose of this endeavor is, ultimately, to establish a better understanding of the physical processes that take place during the SCT and determine the combination of parameterization schemes that best represents them in model simulations.

2. Theoretical background

2.1 Cold Air Outbreak

2.1.1 Climatological and Meteorological Features of CAOs

During a cold air outbreak (CAO), cold air generated in the polar cap spreads out equatorward and surges over the warmer continental or marine surfaces (MCAO) of the mid-latitudes (areas between 35° and 55°N) (Walsh et al, 2001). MCAO episodes are more frequent and severe in the north hemisphere and are mostly recorded during winter (Fletcher et al., 2016) (Figure 2.1). CAO cases are particularly damaging to the agricultural sector (Rogers and Rohli, 1991), as well as water pipes, buildings and other infrastructural components causing significant economic losses especially in regions with warmer climate. Additionally, CAOs are often related to human fatalities. An average of 30 deaths per year in North America is attributed to extreme cold waves, according to the National Weather Service's records that date back to 1989, with the estimated global annual average death rate reaching the order of hundreds or even thousands.

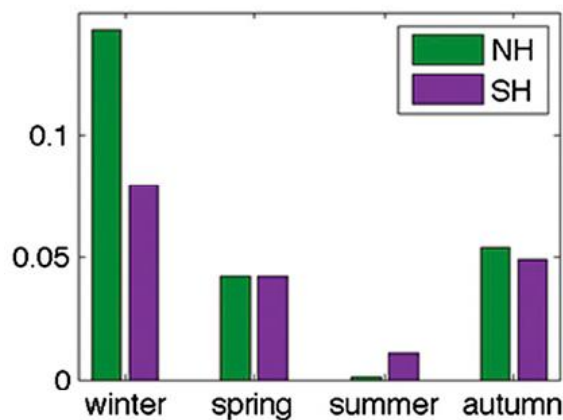


Figure 2.1 Relative Frequency of Occurrence (RFO) of MCAOs in the Northern and Southern Hemispheres (Fletcher et al., 2016).

Recent studies (Thompson et al., 2002; Cai and ren, 2007; Scaife et al, 2008; Kolstad and Scaife, 2010) have argued that CAOs are possibly linked to stratospheric phenomena, such as the Sudden Stratospheric Warming (SSW), in which the stratospheric polar vortex is weakened due to the breaking of upward propagating planetary waves, which could even cause the zonal flow to reverse in extreme cases. Such a disruption of the upper atmospheric circulation causes the polar jet stream to oscillate (Figure 2.2) and allows the southward displacement of cold masses (Kidston et al., 2015). During their southward migration, the air masses undergo sinking, releasing potential energy, which is required to maintain the kinetic energy of the

general circulation, and exchanging heat and vorticity with the ambient air (Matsumoto et al., 1963). The diabatic heating of the air near the surface, due to the increased sensible heat fluxes, causes the lower tropospheric layer to become unstable, which is a clear indication of the occurrence of a CAO event. Fletcher et al., (2016), among others (Kolstad et al., 2009, Papritz et al., 2015) noticed that they could use lower tropospheric instability as a way to detect MCAOs. For that purpose they developed a quantitative expression of lower tropospheric instability, the MCAO index ($M = \theta_{SFC} - \theta_{800}$), which they utilized to define MCAOs as incidents with $M > 0$.

MCAOs are often associated with baroclinic weather systems, characterized by cold surface anticyclones located to the west of warm midlatitude cyclones (Wheeler et al., 2011) which are responsible for the southward (northward) flow in the Northern (Southern) Hemisphere. Severe events are accompanied by a strong upper-level trough that typically displays a mere west-ward baroclinic tilt, implying that the surface low pressure systems are still in the growing phase. The trough is expected to deepen over the course of the first 24h of the incident and decay in the subsequent 24h although it's not unlikely for MCAOs in the Northern Hemisphere to be more persistent (Fletcher et al. 2016).

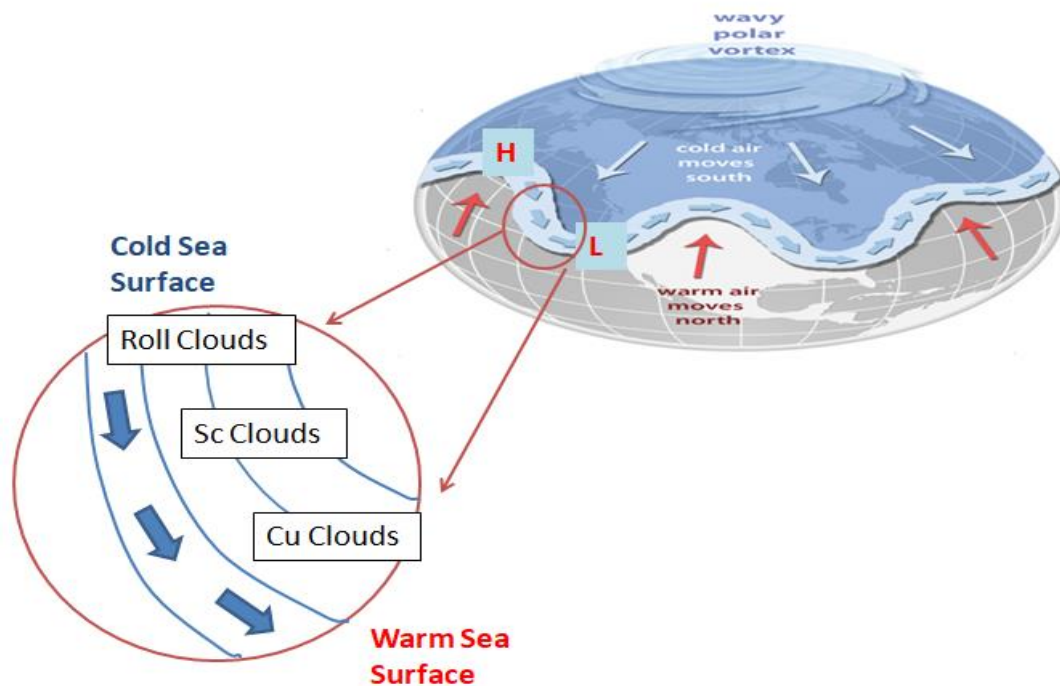


Figure 2.2 Image of the oscillated polar jet stream obtained from noaa.gov and the advection of cold air masses over the warm ocean in the midlatitudes (circled region).

2.1.2 Planetary Boundary Layer Structure and Cloud Cover

In CAO cases, polar continental air masses, prior to their equatorward relocation, are stably stratified and cloud free. The absence of clouds in that area is mostly attributed to the stability conditions that suppress vertical air movements, as well as to the significant large-scale subsidence that due to the descending air of the polar cell. As the air is advected over the warmer sea surface, the enhanced heat and vapor fluxes activate convective processes and therefore, cloud formation. Typically, clouds appear in the pattern of elongated roll-like streams parallel to the direction of the air flow, often referred to in literature as cloud streets (Atkinson et al, 1996). Further, the boundary layer deepens from a few hundred meters to 1-2 km downstream of the point where MCAO index reaches its maximum. As a result, cloud pattern changes, forming into extensive stratocumulus sheets, most likely of open or closed cellular structure (Figure 2.3).

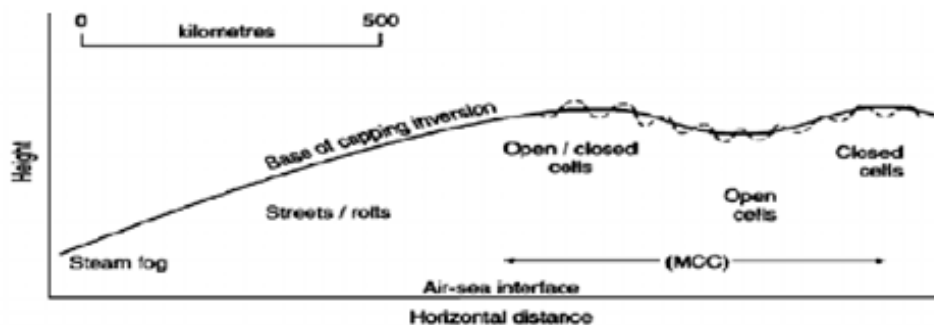


Figure 2.3 cross-section of change in cloud regime along the path of an MCAO (Agee, 1987).

Each of the different patterns encountered in stratocumulus sheets corresponds to a different radiative and climate forcing. This motivated researchers to establish a qualitative and, when possible, quantitative understanding of the factors that determine the cloud cover in stratocumulus overcast areas, as well as to figure out ways to incorporate them in their simulations.

Convection in stratocumulus regimes is mainly driven by long-wave radiative cooling at the cloud top which generates and maintains turbulence and supplies the stratocumulus layer with moisture from the sea-surface increasing its liquid water content (LWC). Entrainment of the overlying, dry, atmospheric air along with the formation of precipitation can cause the cloud to thin or completely dissipate, therefore leading to notable changes in the cloud morphology.

The entrainment rate is strongly dependent on surface fluxes and the strength of the capping inversion, with slower entrainment rates corresponding to stronger inversions. In areas with significant large-scale subsidence, resulting from

convergence in the upper atmospheric levels as encountered in high pressure systems, the descending air is heated adiabatically reinforcing the inversion. However, studies on the effect of subsidence on the formation and life span of stratocumulus clouds have so far been inconclusive, with some claiming that stronger subsidence is expected to increase cloud water (Young et al., 2018) and others that it could, slightly, negatively affect LWP by pushing down the cloud top (van der Dussen et al., 2016).

In CAO events, the dynamic and thermodynamic conditions are constantly changing along the air path thus, transitions between different cloud structures are fairly common. One of the most recent, note-worthy studies was the examination of the transition from closed-to-open-to-closed cells by Feingold et al. (2015). They concluded that open-to-closed cell transition is disproportionately slower because it requires the suppression of rain, the replenishment of aerosol in sufficient concentrations to generate LWP through the process of radiative cooling, whose intensity is proportional to LWP. The investigation of these kinds of transitions, either through observation or simulation, is of great interest for future research.

Finally, the simultaneous effect of increasing sea surface temperature(SST) and boundary layer deepening (Bretherton and Wyant, 1997), radiative heating of the cloud layer (Slingo et al., 1982) as well as evaporative cooling of the air below the cloud base could result to the decoupling of the boundary layer (Abel et al., 2017, Yamaguchi et al., 2017). During the decoupling, the boundary layer is transformed to a two-layer structure, resulting in the detachment of the cloud from the surface heat and moisture fluxes. This mechanism plays a key role in the initiation of a different type of change in cloud morphology, the stratocumulus-to-cumulus transition (SCT) which is discussed in detail in section 2.

2.1.3 Future Projections for CAOs

The factors that determine the time of the season that CAOs frequently occur are the area's latitude and the maritime influence. The duration and magnitude of the event, as well as its spatial extent, strongly rely on the time of the season it occurs (Smith et al, 2018). Most cases are observed in the Northern Hemisphere and are more frequent in Europe, Central Eurasia and North America. The results from a study conducted by Smith et al. (2020), using two different climate reanalysis datasets from 1979-2018, show that CAOs have decreased over time in spatial extent, frequency, duration and magnitude globally, especially in places like Alaska, Canada and the North Atlantic while there has been a rise in cases in Eastern Europe, Central Eurasia and the Southern Ocean.

Frequency and intensity of CAOs are expected to diminish in the following years, in response to global warming (Vavrus et al., 2006) as the temperature of the air will rise more rapidly than the temperature of the oceanic surface, minimizing the surface

fluxes. Regions with strong MCAOs will move poleward, following the receding sea-ice surface (Kolstad, 2007).

Another interesting development related to global warming is the predicted upward shift of the isotherms and the subsequent replacement of ice particles with liquid drops in the CAO clouds, which will make them more reflective to shortwave radiation. According to Murray et al. (2021), this is expected to have a negative feedback on climate (Figure 2.4a,b). However, in the presence of INPs (ice nucleating particles), ice production could still take place despite the increased temperatures. Consequently, an increase in INP concentrations could entirely counteract the rising temperatures and result in further glaciation of the clouds, which would positively feedback on climate (Figure 2.4c). Establishing better knowledge on INP sources, through observations and simulations, as well as their effect on cloud dynamic and microphysical processes (i.e. Secondary Ice Production) is vital for future research and international policy making.

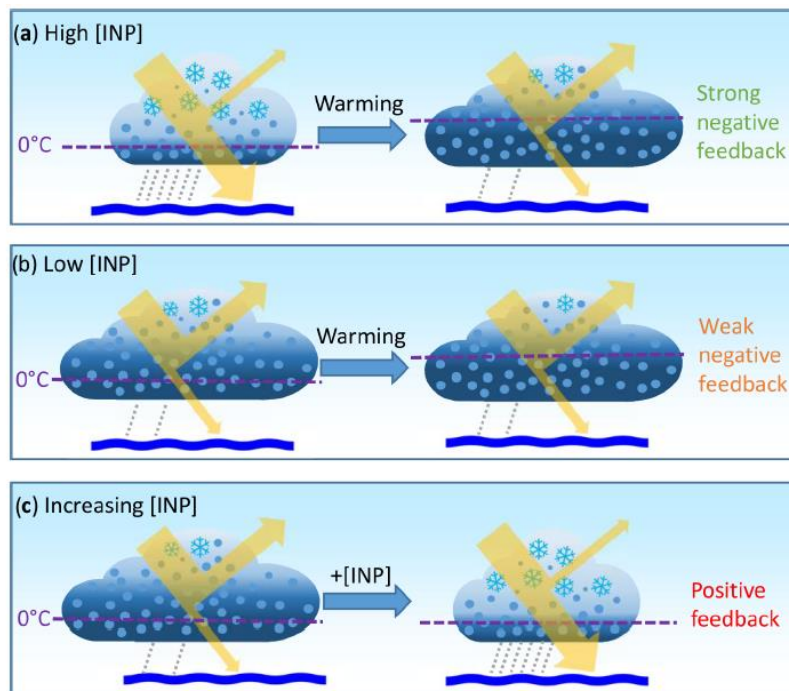


Figure 2.4 Cloud-Phase Climate feedback in different INP concentration scenarios (Murray et al., 2021)

2.2 Stratocumulus to Cumulus Transition

Past studies (Atkinson, 1996; Chung, 2012; Sandu and Stevens, 2011), based on both observations and simulations of CAO cases, have indicated that the most common reason for change in cloud cover is the Stratocumulus to Cumulus Transition (SCT), which is the subject of this study. This phenomenon, despite its frequent occurrence and significance is, to this day, poorly understood and therefore underrepresented in general-circulation and climate models. The SCT bears many

similarities with the closed-to-open cells transitions; both are spotted over areas with increasing SST and are preceded by the warming and deepening of the boundary layer and the depletion of LWC by precipitation. The difference in this case is that, in order for the transition to be activated, the decoupling of the boundary layer is required. The transition is completed with the formation of shallow cumulus clouds that penetrate and detrain into the stratocumulus cloud, enabling its dissipation (figure 2.5).

A number of conflicting theories have been developed over the past decades, in an effort to determine the driving factor of the boundary layer decoupling and, consequently, the SCT. Early studies on the SCT over oceanic areas (Krueger et al., 1995, de Roode and Duynkerke, 1997) drew the connection between decoupling and SCT and noted that the advection of a cold air mass over warm water is, in itself, sufficient to cause decoupling and trigger the transition. This was supported by Lewellen's (1996) prior work that correlated the occurrence of decoupling with increased moisture fluxes. Finally, Bretherton and Wyant (1997) summarized and organized those notes into a coherent theory, in which they argue that the fundamental cause for SCT is the increased surface fluxes while the role of precipitation is complementary.

According to Bretherton and Wyant's study, the increased SST values lead to the deepening of the boundary layer and increase the transport of moisture from the surface to the cloud, which causes the buoyancy fluxes in the cloud layer to spike due to the release of latent heat during water phase changes. At the same time, higher SSTs contribute to the warming of the sub-cloud layer and the weakening of the cloud capping inversion which leads to additional heating by entrainment and drying of the cloud top, which causes the boundary layer mixing driven by radiative cooling to diminish. As a result, a prominent buoyancy flux jump is formed between the in-cloud and sub-cloud layers, with the minimum value (often negative) being recorded just below cloud base.

The mechanism described above is often referred to, in literature, as buoyancy reversal. Xiao et al. (2011) explains that buoyancy reversal occurs when descending air masses become positively buoyant before they reach the updraft condensation level. This asymmetry between ascending and descending masses is caused by the surface latent heat enhanced fluxes that generates in-cloud buoyancy fluxes strong enough to overpower the stratocumulus-top radiative cooling

The contribution of the increasing SST values in triggering shallow cumulus convection is undisputed. However, recent studies have shown that evaporative cooling of the precipitating drizzle below the cloud base is necessary in order to promote decoupling and initiate the stratocumulus-to-cumulus transition. Yamaguchi et al. (2015), after noticing a strong modulation in the SCT theory caused by precipitation in their control run, proceeded to conduct a set of additional LES simulations (2017), using a bulk, two-moment microphysics scheme to further

investigate the influence of drizzle on the marine boundary layer structure and, effectively, the transition. They maintained that the diabatic warming through drizzle condensation in the cloud layer and the cooling of the underlying air due to evaporation of the precipitating drizzle, created a stable layer right below the cloud-base that isolated the stratocumulus cloud from the surface fluxes. Therefore, moisture and aerosol accumulated in the unstable surface layer, where scattered cumulus clouds started to appear and penetrate through the conditionally unstable layer and eventually the Stratocumulus cloud. The detrainment of the air from the cumulus tops accelerated the Sc cloud break-up, although, the injection of cloud and rain droplets, as well as high aerosol concentrations by the rising cumulus into the stratocumulus layer was considered, by Yamaguchi, as instrumental in draining the stratiform cloud and reducing the cloud cover. Finally, Yamaguchi highlighted the importance of using prognostic to predict aerosol concentrations, in order to allow a natural evolution through collision-coalescence and precipitation and therefore avoid the biases in SCT simulations.

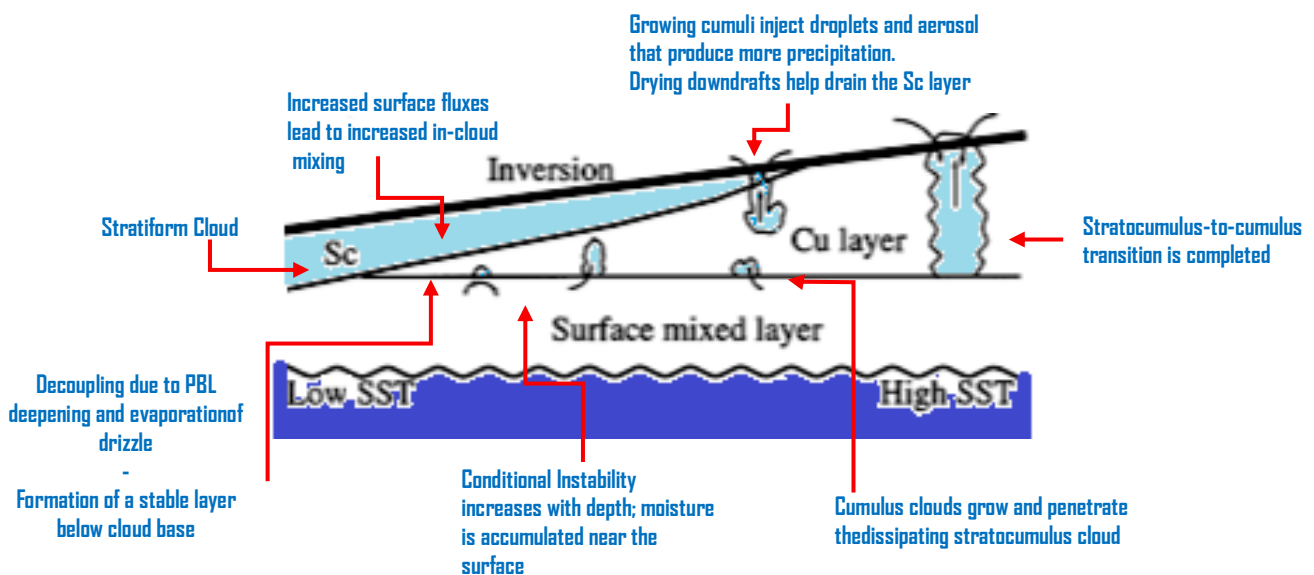


Figure 2.5 Schematic representation of the processes that take place during the Stratocumulus-to-Cumulus transition (Wyant, 1997).

Yamaguchi’s theory was in agreement with Abel et al. (2017) who, in their own SCT study, claimed that the boundary layer decoupling was precipitation-induced and that the increase of SST could not single-handedly produce sufficient cloud break-up. They also presumed that the Hallett-Mossop (1974) mechanism, also known as rime-splintering, which is enabled by the lowering of the cumulus clouds’ base, plays a major role in the generation of precipitation.

2.3 Cloud Microphysical Processes

As discussed in previous segments, the evaporation of precipitating particles is considered to be largely responsible for the decoupling of the stratocumulus-topped boundary layer and therefore plays a key role in the initiation of the stratocumulus-to-cumulus transition. In this context, the accurate representation of the processes controlling the formation and rate of precipitation are of significant value for this study.

Liquid condensate in clouds is produced through the processes of homogeneous and heterogeneous nucleation. A basic requirement for these processes to be implemented is the supersaturation of the ambient air ($S = (RH - 1)100$, where $RH = \frac{e_s}{e_{s\infty}}$ is the Relative Humidity and $e_s, e_{s\infty}$ the saturation of the air adjacent to and away from the surface of the droplet). Supersaturation is typically obtained by the ascent and adiabatic cooling of moist air parcels (Wallace and Hobbs, 2006). In homogeneous nucleation, water molecules collide to form small embryonic water droplets. The fate of these droplets is determined by their effective radius; droplets whose initial size is larger than a critical value (r_c) are due to spontaneously grow by condensation while smaller droplets will evaporate. The critical radius value (r_c) is obtained by the Kelvin equation:

$$r_c = \frac{2\sigma}{nkT \ln\left(\frac{e}{e_s}\right)}$$

, where σ is the surface tension of the droplet, T is the temperature, n is the number of moles, e is the partial vapor pressure and e_s is the saturated vapor pressure of the system.

Homogeneous nucleation is not the governing process in the formation of natural clouds. Liquid droplets formed by chance collisions of water molecules are rarely larger than $1\mu\text{m}$ and therefore require high supersaturation levels in order to grow in size. Instead, the majority of liquid hydrometeors are produced by condensation of the excess water vapor on atmospheric aerosol also known as Cloud Condensation Nuclei (CCN). This process is also referred to as heterogeneous nucleation. Larger atmospheric particles are more effective in activating droplets since the critical radius value is more easily exceeded.

Another factor that shapes the process of heterogeneous nucleation is the solubility of particles that act as condensation nuclei. When water condenses on the surface of a soluble in water particle, the particle dissolves wholly or partly, leading to the formation of a solution droplet. In identical temperature conditions and below a certain droplet radius, relative humidity adjacent to a solution droplet is less than that

encountered in the proximity of a pure water droplet and, therefore, the growth of the droplet is favored.

The evolution of solution droplets is best described by the Köhler curves theory. As it is demonstrated in figure 2.6, droplets produced by particles of different chemical compositions are likely to follow different paths. If during the growth of the solution droplet (e.g. NaCl), the supersaturation adjacent to it, even at its peak value, doesn't surpass the ambient air supersaturation, the droplet will continue to grow, eventually forming a cloud drop. Droplets that have passed over their Köhler curve peak are said to be activated. In the opposite case (e.g. $(\text{NH}_4)_2\text{SO}_4$), when the supersaturation adjacent to the formed solution droplet becomes equal to the ambient air supersaturation before reaching the peak in its respective Köhler curve, the growth ceases. These droplets are referred to as unactivated or haze droplets.

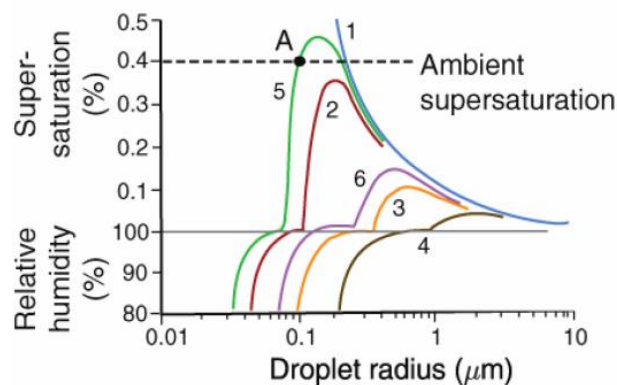


Figure 2.6 Köhler curves of solutions droplets containing 10^{-19} kg of NaCl (red curve), 10^{-18} kg of NaCl (orange curve), 10^{-17} kg of NaCl (brown curve), 10^{-19} kg of $(\text{NH}_4)_2\text{SO}_4$ (green curve), 10^{-18} kg of $(\text{NH}_4)_2\text{SO}_4$ (purple curve) and a pure water droplet (blue curve). The dashed line represents ambient air supersaturation (figure 6.3 in Wallace and Hobbs, 2006).

The activated droplets will eventually grow to the size of rain drops by diffusion or collection. The diffusional growth rate is inversely proportional to the droplets' radius, therefore growth by diffusion diminishes over time, as drops grow bigger (figure 2.7). Larger cloud drops develop higher terminal velocities which causes them to collide with smaller droplets that are lying in their path and increase their size by collecting them. Turbulence within the cloud layer reinforces the aforementioned cloud growth processes since high vertical velocities are related to increased supersaturation rates and collision-coalescence efficiency. Consequently, precipitation is produced quicker in deep clouds with strong updrafts (cumulus) than in thin clouds with weak vertical in-cloud mixing.

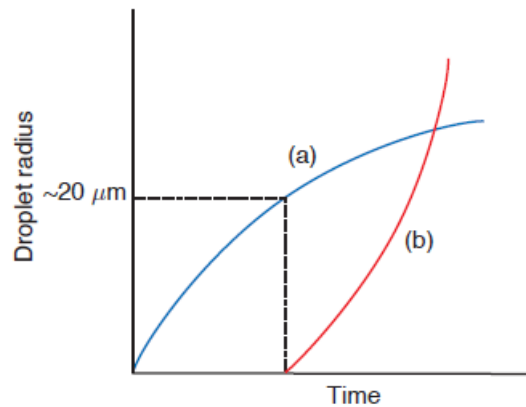


Figure 2.7 Droplet growth rate by diffusion (blue curve) and collection (red curve) (figure 6.15 in Wallace and Hobbs, 2006).

Clouds that are observed in CAO cases are typically mixed-phase, due to the characteristic low temperatures (below zero) that favor the production of cloud ice. In absence of foreign particles, cloud ice could be formed through homogeneous nucleation. The number and size of embryonic droplets formed by chance aggregations increases with decreasing temperature, therefore ice production by homogeneous nucleation is more common in high clouds, at temperatures lower than $[-33^{\circ}\text{C}]$ (figure 2.8). However, the freezing of a supercooled cloud droplet could also occur in much higher temperatures too, with the involvement of a special category of atmospheric particles called Ice Nucleating Particles (heterogeneous nucleation). INP concentrations are higher in the northern middle to high latitudes, where MCAO activity is stronger. This could be explained by the proximity of those regions to terrestrial sources, such as pro-glacial deposits (Bullard et al., 2016; Prospero et al., 2012) and dust from Iceland's deserts (Sanchez-Marroquin et al., 2020). There is also record of high concentrations biogenic materials of terrestrial (sediments from rivers or vegetated areas) (Tobo et al., 2019; Conen et al., 2016; Schnell and Vali, 1976) and maritime origin (sea-water aerosolized through the actions of waves and bubble bursting) (Schnell, 1977; Schnell and Vali, 1975; Wilson et al., 2015; Irish et al., 2019; DeMott et al., 2016; Irish et al., 2017; Creamean et al., 2019) that are highly active even at the highest temperatures.

If one of these particles is already contained in the droplet, water molecules gather onto the surface of the particle forming an ice-like structure that could potentially grow and cause the entire droplet to freeze. Pure water droplets could even freeze at higher temperatures through contact nucleation, after colliding with particles called contact nuclei. Finally, ice could be generated directly from the vapor phase through deposition on certain particles at low enough temperatures, as long as the air is supersaturated with respect to ice.

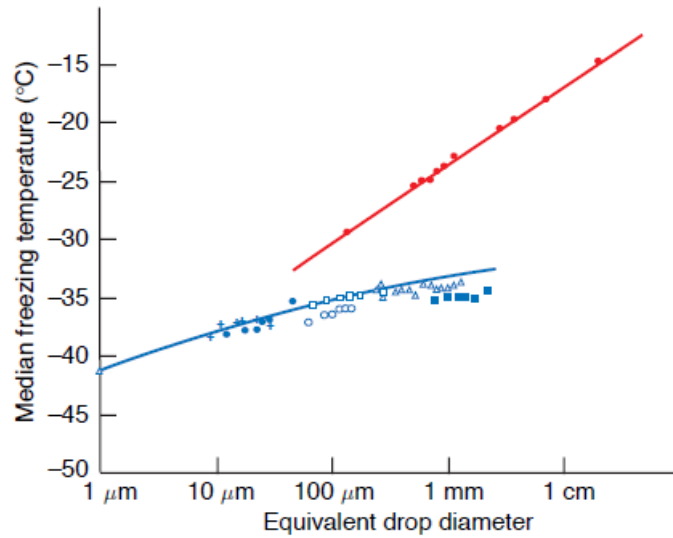


Figure 2.8 Median freezing temperatures of water as function of their equivalent drop diameter. Blue symbols represent homogeneous freezing while red symbols represent heterogeneous freezing (figure 6.29 in Wallace and Hobbs, 2006).

In cold clouds, air supersaturation with respect to ice is much greater than supersaturation with respect to liquid water, which causes ice particles to grow in a much faster pace than liquid droplets (growth by deposition). Collisions of frozen hydrometeors with each other (aggregation) or with supercooled liquid drops that freeze onto their surface (riming) also contribute to their growth. Much like the mechanism of growth by diffusion in the case of liquid droplets, growth of ice crystal by deposition decelerates as particles become larger, whereas growth by aggregation and riming intensify. As ice particles become successively bigger, their terminal velocities increase and they start settling. During their fall, as they come in contact with the warmer underlying air, they often melt and eventually reach the surface in the form of rain. Therefore, it's reasonable to conclude that cloud ice production processes are largely responsible for the formation of precipitation in mixed clouds.

In homogeneous and heterogeneous nucleation, ice particles are formed by water or vapor, therefore they're characterized as primary nucleation processes. In natural clouds, however, it has been observed that ice particle number concentrations exceed by several orders of magnitude the number concentrations of ice nuclei, even in situations where ambient temperatures are too high to excuse enhanced homogeneous nucleation. Over the last decades, several theories have been developed aiming to identify new mechanisms that could potentially amplify primary nucleation processes, in order to explain this discrepancy between expected and measured values of ice particle concentration. A few examples of such mechanisms are the thermophoretically enhanced contact freezing (Beard, 1992, Young et al., 1974, Hobbs and Rangno, 1985) and pre-activated INPs (Beard, 1992, Fridlind et al., 2007). Recent studies have made a compelling argument for a potential affiliation between the excess cloud ice particles and Secondary Ice Production (SIP) mechanisms, through which new ice crystals are being produced in the presence of preexisting

cloud ice, without the involvement of INPs or homogeneous freezing (Field et al., 2017). Following in that path, this study will test and evaluate the contribution to the initiation of the SCT of the following SIP processes:

- Hallett-Mossop mechanism / rime splintering: It's the process that has received the most scientific attention in the past decades. A number of researchers (Hallett and Mossop 1974; Choulaton et al. 1980; Heymsfield and Mossop 1984; Saunders and Hosseini 2001) have experimentally studied this effect using variations of the same set-up of an ice coated cylinder rapidly rotated in a cold chamber containing supercooled liquid drops. All the above studies have agreed that the general requirements for this process to take place is a) the air temperature to be within the $[-8, -3]$ °C range and b) the droplets involved in the process to be larger than ~ 25 μm or smaller than ~ 13 μm in diameter that can freeze upon their collection by ice frozen particles like rimed aggregates, graupel or large frozen drops. The liquid droplets, during their accretion on the surface of large ice particles, break up into splinters due to a build-up of internal pressure strong enough to crack the frozen shell, letting the unfrozen liquid to escape (Visagie, 1969, Mossop et al., 1974). Griggs and Choulaton (1983) and Mason (1996) suggested that the ice shell is too strong to break at temperatures lower than -8 °C. Dong and Hallett (1989) maintained that the splintering was caused by the thermal shock induced by the temperature gradient between substrate and drop. Choulaton (1980) noted that larger drops (>25 μm) are more likely to freeze symmetrically and produce splinters when smaller drops freeze on top of them, due to the narrow neck at the attachment point that limits thermal contact. Mossop (1985) argued that the minimum impaction speed required, between liquid drops and ice particles is 0.2 m/s while collision velocities that are related to peak splinter production are within the 2-4 m/s range. Saunders and Hoseini (2001) found that rime splintering peaks at higher impaction speed values (~ 6 m/s).
- Droplet Shattering/Fragmentation: Freezing drops within the radius range of $[100$ $\mu\text{m} - 1$ $\text{mm}]$ could potentially shatter producing a large amount of new ice crystals, a process which largely depends on the temperature at which the freezing of the droplet occurs (Mason and Maybank, 1960). Nucleation of the drop at a temperature $-T_f$ °C causes $T_f/80$ of the droplet's mass to become quickly solidified while the latent heat of fusion causes the temperature of the entire drop to rise to 0°C. Partial freezing of the drop is initiated around the surface and spreads radially inwards in the form of dendritic crystals, at a pace dictated by the dissipation of latent heat to the environment. The amount of air contained in the droplet, which also depends on the nucleation temperature, is another determining factor in the shattering of the freezing drop. In the case of a slightly supercooled droplet heterogeneously nucleated by an ice crystal, the very small quantity of air can escape to the environment and a thin, transparent shell is formed. Weak spots of the frozen surface could potentially be ruptured

under pressure of the solidifying interior causing the extrusion of liquid and the formation of spikes. If the shell is too strong to be ruptured, large stresses develop leading to the explosion of the frozen drop in two or more fragments and the production of a large amount of splinters. At lower nucleation temperatures, larger amounts of air are released in the droplets and trapped in the ice, creating a porous texture that enables the expansion of the freezing drops and the extrusion of the liquid from the interior, preventing their fragmentation and splintering.

- Collisional Fragmentation/Breakup: In natural clouds, collisions can be distinguished into two categories, the first being random collisions caused by vertical and horizontal wind shear and the second being ordered collisions, caused by the difference in terminal velocity between particles of different sizes and shapes (Vardiman, 1978). Both types of collisions between ice particles can lead to fragmentation and thus, secondary ice production. Random collisions are believed to outnumber ordered collisions in highly turbulent cloud conditions, they are difficult to adequately quantify and formulate in an analytic manner. In order to predict ordered collisions, one had to take into account the number concentrations, sizes, shapes and vertical velocities of different crystal types. Some of the factors that regulate the amount of ice fragments produced by such collisions are the masses of the two colliding particles, the contact time of their collision, the coefficient of restitution etc. Due to difficulty in observation and great variability of these variables, researchers often use the kinetic energy of impact and the change in momentum as indicators for the quantity of new ice produced.

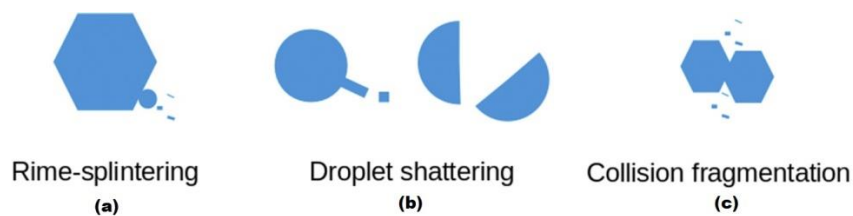


Figure 2.9 Schematic representation of secondary ice production mechanisms (Field et al, 2017).

Scientific opinions on the impact of secondary ice production processes on the formation of surface precipitation are conflicting. Change in ice crystal number concentrations could extend cloud duration and delay precipitation. However depositional growth of the additional particles may also deplete supersaturation levels to a point where the Bergeron process initiates, ice hydrometeors become larger and precipitation is accelerated (Figure 2.10). Connolly et al. (2006) did not detect any significant changes in the rate of precipitation from a tropical thunderstorm after they altered the rime splintering mechanism in their WRF simulations. Dearden et al (2016) agreed that growth by deposition was much more influential in the formation of precipitation than rime splintering. On the other hand Clark et al. (2005) claimed

that surface precipitation is modified by the implementation of SIP processes due to additional latent heating which affects the vertical temperature profile. Taylor et al. (2016) highlighted the significance of SIP, in combination with droplet coalescence, in determining precipitation timing and intensity in maritime cumuli. Glassmeier and Lohmann (2016) argued that the effect of SIP could even reduce the sensitivity of precipitation to aerosol perturbations. In a more recent study, Sullivan et al. (2018) concluded that the incorporation of SIP mechanisms in model simulations of a cold frontal rainband increased accumulated precipitation or precipitation rates up to 30%, in areas where these values are largest, with rime splintering being the most influential in the formation of precipitation.

In conclusion, SIP appears to be instrumental in modulating precipitation in natural clouds. Ice-initiated precipitation has been associated with the top 10% of heavier rains according to data from the Tropical Rainfall Measuring Mission (Lau and Wu, 2011). Therefore, there is merit in thoroughly investigating the involvement of SIP processes in the initiation of the SCT, in the following chapters.

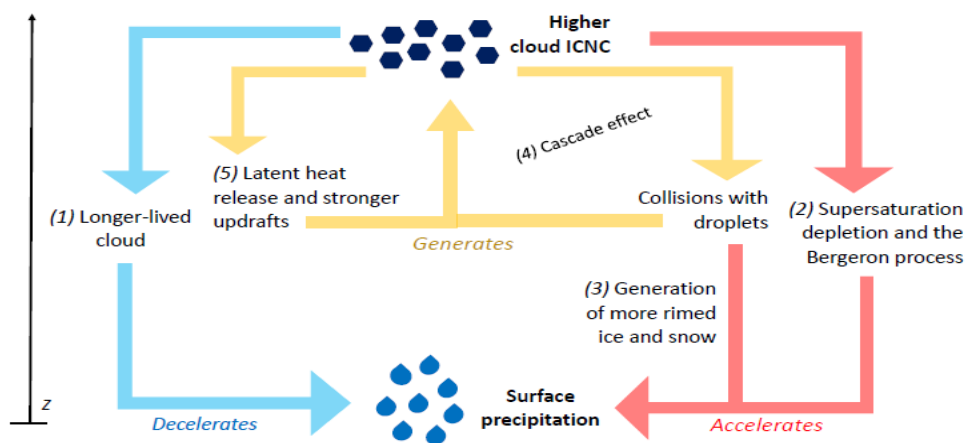


Figure 2.10 Schematic illustration of the different ways in which secondary ice production mechanisms can affect precipitation (Sullivan et al, 2018).

3. Methodology

This study, is mainly based on numerical simulations performed using the Weather Forecast and Research Model (WRF). Also, aircraft data collected northern of Scotland and near the Norwegian coastline on 24/11/2013, were used for the needs of this study. A brief description of the campaign is given by Abel et al. (2017).

3.1 Area of study and prevailing atmospheric conditions

The CAO event we are studying took place on the north of the United Kingdom during December 2013. During this campaign Abel et al. (2017) managed to capture a stratocumulus-to-cumulus transition near the Norwegian coastline. The Facility of Airborne Atmospheric Measurements (FAAM) BAe-146 research aircraft took flight at 0700 UTC on 24/11/2013 from Prestwick airport in Scotland and followed a multi-level, multi-hour trajectory, exploring several cloud profiles across the area of the transition. There was also a series of below cloud and at cloud base level runs followed by a series of vertical sampling at altitudes from close to the sea surface to above the inversion at the top of the marine boundary layer. Part of the flight track close to the transition is shown in Figure 3.1a (obtained from Abel et al. 2017, figure 2c) where the midpoints of the vertical profiles (P1-P9) are also pictured.

An AMSR2 satellite image of the LWP horizontal distribution during the event is presented in Figure 3.1b (Figure 2a from Abel et al., 2017). The LWP map shows that, in the stratiform area, the LWP values exceeded 300 g/m^2 and then rapidly dropped below 100 g/m^2 when the transition was initiated. The transition area can be observed more closely in the MODIS Aqua true color image (midpoint P8, Figure 3.1a).

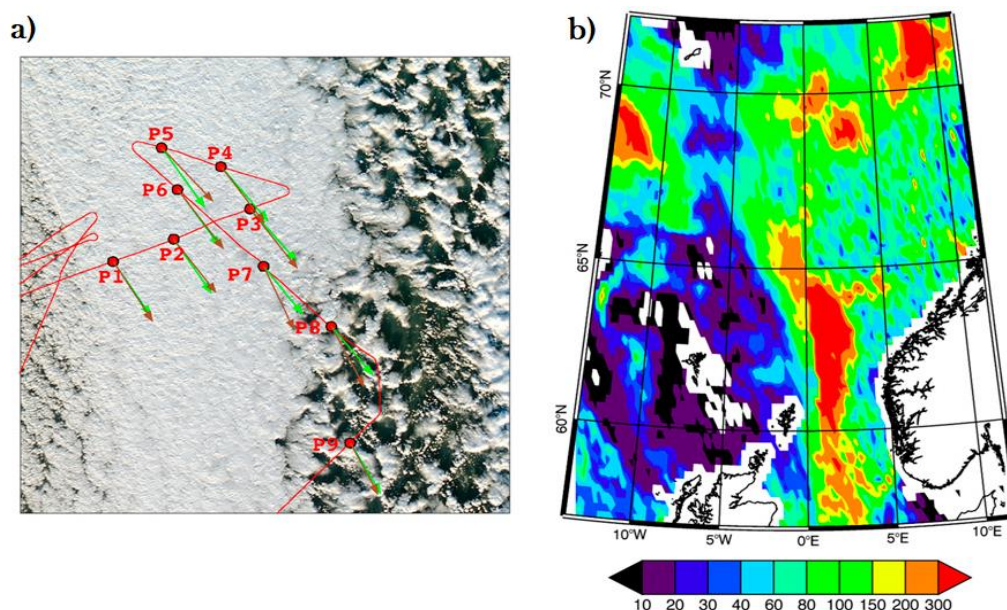


Figure 3.1 a) True-color satellite imagery of the transition area from MODIS Aqua at the time of the transition, with the flight track and midpoints of the vertical profiles denoted in red, b) Liquid Water Path (gm^{-2}) satellite measurements of the area of study at the time of the SCT event from AMSR2 (Abel et al, 2017).

3.2 Aircraft Measurements

The measurements from Abel et al.'s (2017) experimental campaign that we used for the evaluation of our simulations' results are presented in Table 3.1.

Table 3.1

Aircraft Measurements	
Measured Variable	Instrument
Air temperature (K)	Rosemount/Goodrich type 102 total air temperature sensor
Wind velocity (ms^{-1})	AIMMS-20 probe
Hydrometeor $>100 \mu\text{m}$ number concentration (cm^{-3})	CIP-100 probe (Baumgardner et al., 2011)
Liquid Water Content (gm^{-3})	Nevzorov probe (Korolev et al., 1998)
Liquid Water Path (gm^{-2})	MARSS radiometer (McGrath and Hewison, 2001).

3.3 Simulations

Simulations for the needs of this study were performed using the Weather Forecast and Research Model (WRF), version 4.0.1, which features two dynamical cores, a data assimilation system, and a software architecture supporting parallel computation and system extensibility (NCAR, Mesoscale and Microscale Meteorology Laboratory, <https://www.mmm.ucar.edu/weather-research-and-forecasting-model>).

The dynamical solver selected for our application is the ARW core (Advanced Research WRF) which includes the non-hydrostatic Euler equations, a terrain following vertical coordinate and Arakawa C-grid staggering. The model includes a plethora of parameterization schemes, numerical and dynamical options and allows the incorporation of phenomena of different scales with options for domain nesting and time splitting. The model's structure is depicted in Figure 15.

WRF Modeling System Flow Chart

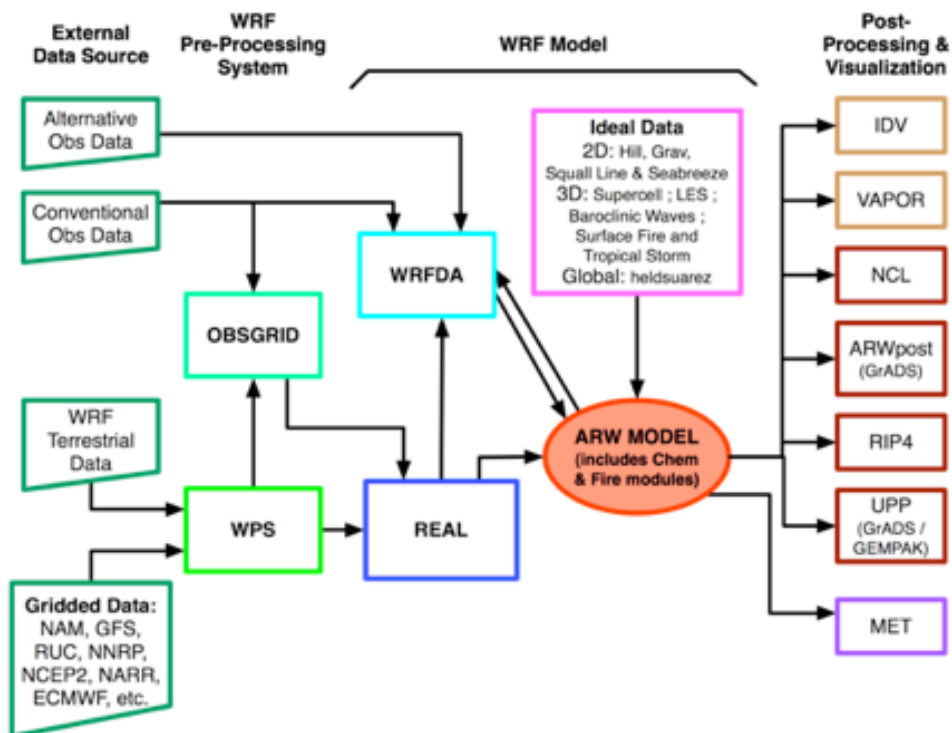


Figure 3.2 WRF model flow chart. (ARW, Version 4 Modelling System User’s Guide, January 2019)

For this application, we have considered 3 domains nested within each other, with grid resolution ranging from 9km in the parent domain to 1 km in the smallest domain (Figure 3.3). More information on the setup can be found in Table 3.2 while the parameterization schemes used are listed in Table 3.3. The model’s initial state and upper and lateral boundary conditions were generated using the ERA5 re-analysis dataset (<https://cds.climate.copernicus.eu/cdsapp#!/dataset/reanalysis-era5-pressure-levels?tab=overview>).

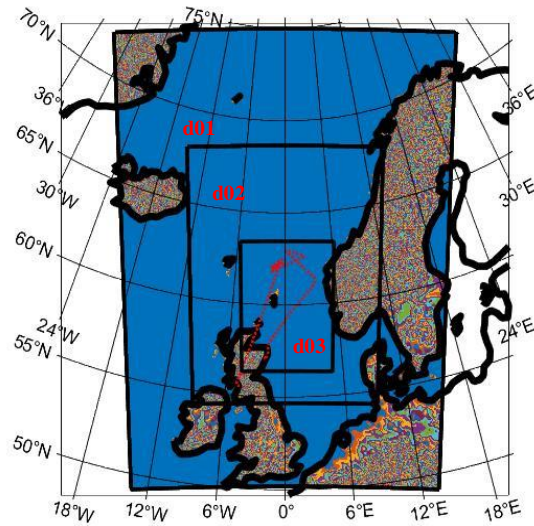


Figure 3.3 Domain distribution in WRF simulations.

Table 3.2

Model Set-up			
	Domain 1	Domain 2	Domain 3
Horizontal Domain Size (west-east)	2088 km	1254 km	592 km
Horizontal Domain Size (north-south)	2781 km	1677 km	778 km
Grid size	9 km	3 km	1 km
Outer Domain center	latitude: 62.25° longitude: 0°		
Air pressure at the top	10 hPa		
Number of vertical levels	70 (29 of them corresponding to altitudes lower than 3 km)		
DZ_{min}	15 m		
DZ_{max}	1200m		
Map projection	polar		

Table 3.3

Parameterization schemes	
• Microphysics :	<i>Morrison double-moment scheme</i>

• Shortwave Radiation:	<i>RRTMG</i>
• Long-Wave Radiation :	<i>RRTMG</i>
• Surface Layer :	<i>Revised MM5</i>
• Land Surface :	<i>Noah land surface model</i>
• PBL :	<i>Yonsei University scheme</i>
• Cumulus :	<i>Grell 3D (only in domain 01)</i>

3.3 Microphysics Parameterizations

The inclusion of the microphysical processes that transpire during the formation of clouds is essential for the accurate simulation of the state of the atmosphere. These processes take place in much smaller scales than the size of the resolvable grid in mesoscale and general circulation models. Therefore, representation of the effect of these sub-grid processes is achieved by using resolvable scale fields with the help of parameterization schemes.

In WRF, the microphysical parameterizations are divided in two main categories: bin models, in which the evolution of the particle size distribution is explicitly calculated (Feingold et al. 1994; Khvorostyanov 1995; Stevens et al. 1996; Harrington et al. 1999; Jiang et al. 2001) and bulk models that use a distribution function to represent the size of the different types of hydrometeors (Lin et al. 1983; Rutledge and Hobbs 1983; Dudhia 1989; Ferrier 1994; Walko et al. 1995; Fowler et al. 1996; Meyers et al. 1997; Reisner et al. 1998). The use of bin schemes is rarely preferred, especially in simulations of a considerable length, due to the significant computational cost. In contrast, bulk schemes are more computationally simple but, often, at the cost of their quantitative accuracy.

The deficiency of bulk schemes in accuracy is partly overcome with the prediction of multiple moments (prognostic variables such as mixing ratio, number concentration, radar reflectivity etc.) of the size distribution of various types of particles. Morrison et al. (2005) constructed a double-moment bulk microphysics scheme predicting the mixing ratios and number concentrations of 5 categories of hydrometeors (droplets, rain, cloud ice, snow, graupel).

Each hydrometeor class is represented by a Gamma size distribution of the following form:

$$f(D) = N_0 D^{p_c} e^{-\lambda D},$$

where D is the particle diameter, p_c , λ and N_0 are the spectral index, slope and intercept respectively. Values of p_c for droplets are a function of the cloud and thermodynamic properties and are specified for cloud ice, snow, graupel and rain. Values of λ and N_0 are found by relating the PSD to the predicted variables N and q :

$$N = \int f(D)dD, \quad q = \int m(D)f(D)dD,$$

where $m(D)$ is the mass of each particle.

This study is mainly focused on the ability of secondary ice production processes to produce precipitation and therefore improve the representation of the SCT. Therefore, we have applied the Morrison et al.'s microphysics scheme in combination with various representations of these processes. The scenarios that were tested are listed in Table 3.4.

Table 3.4

Sensitivity Tests	
DSH	droplet shattering mechanism (Phillips et al., 2018)
HMenh	Hallet-Mossop mechanism activated disregarding hydrometeor mass thresholds; parameterization (Atlas et al., 2020)
BR0.2	Collisional break-up mechanism with rimed fraction=0.2 (Phillips et al., 2017)
BR0.4	Collisional break-up mechanism with rimed fraction=0.4 (Phillips et al., 2017)
ALL0.2	Combined effect of all mechanisms (rm=0.2)
ALL0.4	Combined effect of all mechanisms (rm=0.4)

4. Results

The analysis and discussion of the results of the simulations, in comparison to observational data acquired from the experimental campaign of Abel et al. (2017), are presented in this section. We investigate the ability of the WRF model to simulate the cloud characteristics during the stratocumulus-to-cumulus transition, as well as the degree to which the transition is impacted by the inclusion of SIP mechanisms.

The cold air outbreak is properly represented in the WRF simulations as demonstrated in Figure 4.1. A notably cold air mass, originated from the north, can be seen surging over the North Atlantic and the Scandinavian Peninsula on the date of interest (Figures 4.1.1b and 4.1.2.b). The cold air mass appears to correspond to a low pressure system and is slowly advected to the east over the course of the day, being trailed by a high pressure center. The sea surface temperature substantially increases from below 0°C values to 11°C as the air masses approach the shore (Figure 4.1b), creating favorable conditions for the activation of cumulus convection and the initiation of the SCT according to Bretherton and Wyant's theory (1997). This can also be seen in Figures 4.1.1.c and 4.1.2.c where the increased SST-T values indicate significant sensible heat fluxes near the coast.

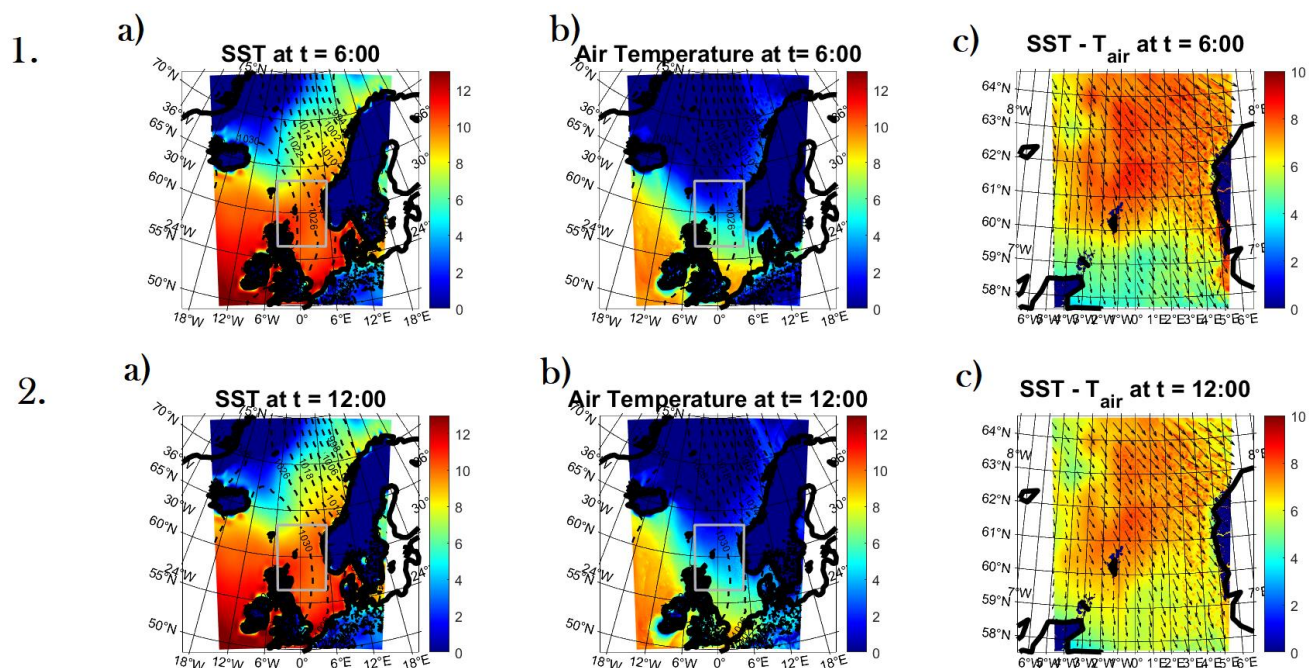


Figure 4.1 Timeframes of the horizontal distribution of **a)** sea surface temperature (SST) and surface atmospheric pressure (contours), **b)** air temperature near the surface and surface atmospheric pressure (contours) **c)** SST-T_{air} (color plot) in domain 03 and wind speed and direction near the surface **1a-c)** at 0600 UTC and **2a-c)** at 1200 UTC.

Figure 4.2 shows the simulated horizontal distribution of liquid water path (LWP) for each of the different scenarios that were tested (as summarized in Table 3.4); the plots correspond to the 1200 UTC timeframe of each simulation to enable the comparison with satellite observations. In the CONTROL simulation (Figure 4.2a), LWP values increase in the mean wind direction, surpassing 300 g/m^2 before the transition. As the transition is initiated, the cloud layer dissipates and LWP values drop, as a result of the boundary layer deepening and the imposed reduction in the number concentration of droplets (from 71.60 cm^{-3} to 13.73 cm^{-3}), in consistence with the satellite observations (Figure 4.2d, obtained from Abel et al., 2017, Figure 2a). However, the point of the break-up is displaced further downwind than the 2.5° meridian which is its observed location (Figure 4.2g, obtained from Abel et al., 2017, Figure 2b). The inclusion of the droplet shattering and enhanced Hallet-Mossop mechanisms (DSH and HMenh run respectively, Figures 4.2e-f) did not affect the cloud properties in the stratocumulus region immensely but did lead to a more defined break-up of the cloud layer in the convective region. In the sensitivity tests where the collisional break-up process was included (BR0.2 and BR0.4 runs, Figures 4.2b-c) there is an evident reduction in LWP in both the stratocumulus and the cumulus area, especially in the BR0.4 case where the LWP values after the transition reveal a vast depletion. However, BR0.4 is the only scenario that accurately predicts the time and location of the transition. It should be noted that, in all cases, the stratocumulus layer is maintained over the area where SST- T_{air} values (and therefore sensible heat fluxes) peak, which confirms Abel et al. (2017) and Yamaguchi et al.'s (2017) theory that rising SST is not solely responsible for the occurrence of the SCT.

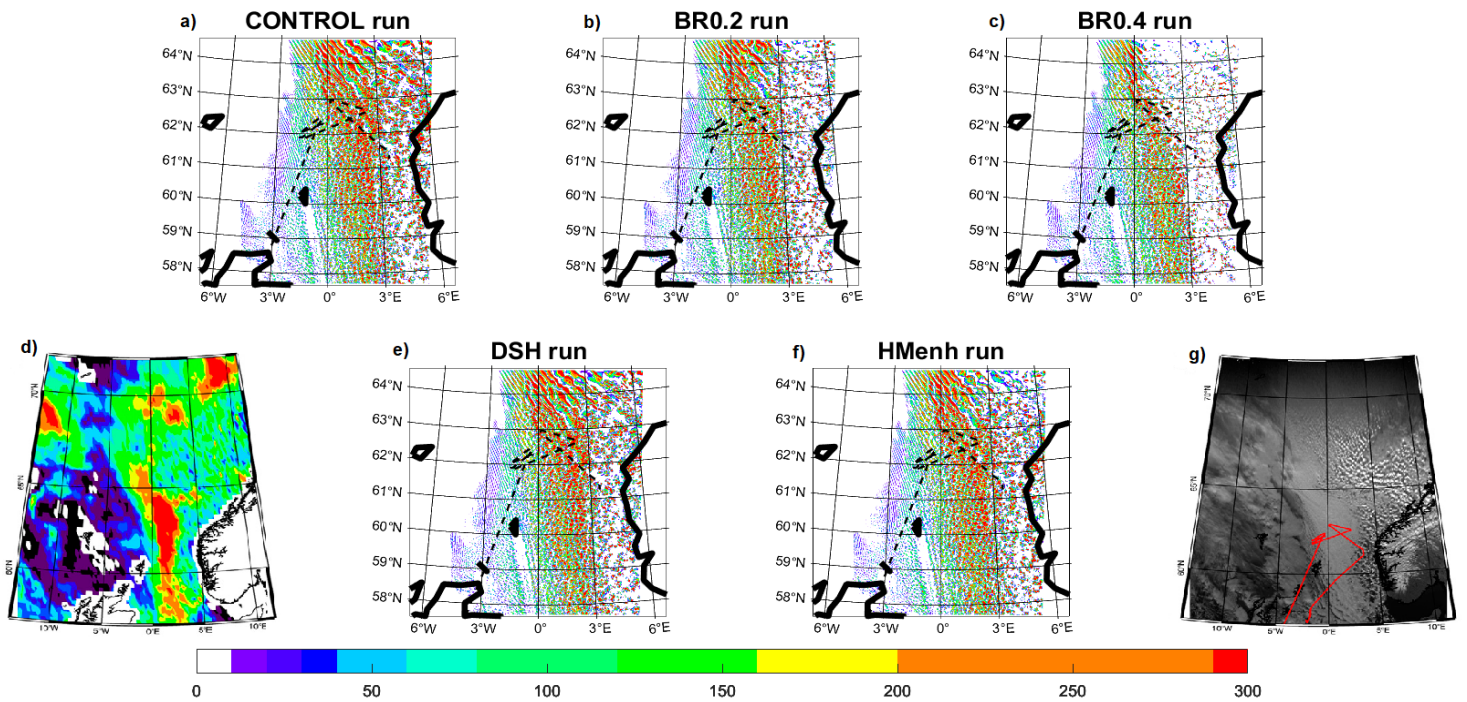


Figure 4.2 Liquid Water Path (LWP) maps of each simulation at 1200 UTC. Values lower than 10 g/m^2 are being ignored in order to enable the depiction of cloud free conditions.

The time-series of LWP values of each simulation along the aircraft trajectory is plotted in comparison to the observational values in Figure 4.3. The CONTROL simulation (Figure 4.3a) provides a better fit to the observational curve in the stratiform region but maintains unrealistically high LWP values even after the transition point which is predicted with a delay of almost 20 minutes. The cloud free areas are narrow and frequently interrupted by exaggerated LWP peaks surpassing 800 g/m^2 . These peaks are relatively smoother and fewer in the DSH and HMenh runs (Figure 4.3b) but the timing of the transition is not notably improved. The collisional break-up of heavily rimed particles (BR0.4, Figure 4.3c) is the most effective in decreasing the cloud's LWP in the cumulus area and simultaneously predicting the correct time of the transition as shown by the immediate drop of LWP that coincides with the aircraft approaching the convective region. However, this is accomplished at the cost of the underestimation of LWP in the stratocumulus area.

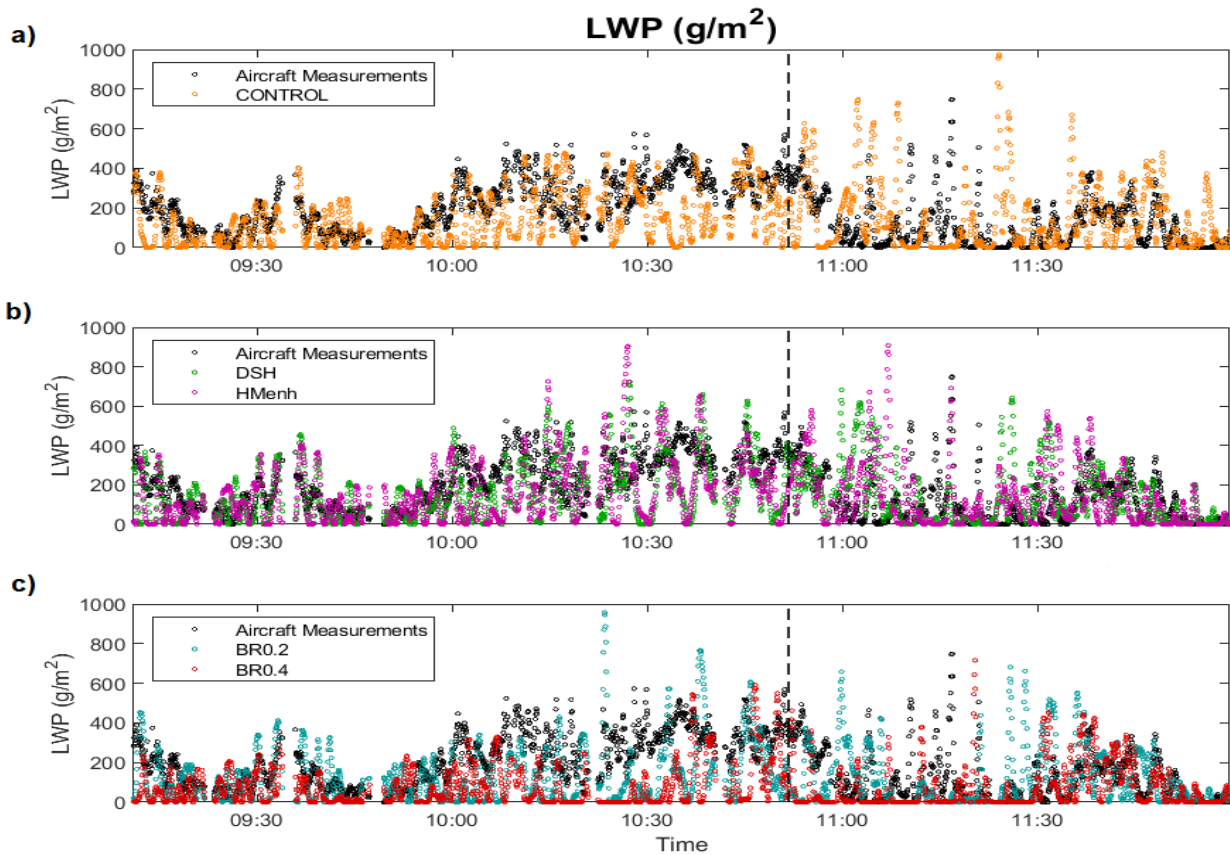


Figure 4.3 Time-series of the simulated LWP values in each scenario and the aircraft measurements along the flight path. The time of the aircraft crosses the cloud transition is denoted with a dashed vertical line.

By plotting the simulated LWC cross sections along the aircraft trajectory (Figure 4.4), it is evident that the heights of the simulated cloud top and base are on average at 2 km and 1 km respectively, in accordance to the observations. Additionally, the deepening of the boundary and cloud layer along the trajectory is accurately represented in all cases. The CONTROL run (Figure 4.4a), in the stratiform region, produces higher LWC values, frequently surpassing 0.4 g/m^3 and 0.6 g/m^3 in some instances. The thickness of the cloud peaks at approximately 1.2 km to the west of the observed point of the SCT. These results are consistent with the aircraft observations (Figure 4.3f), but this scenario fails to adequately simulate the decrease of LWC in the cumulus region. The break-up is displayed more prominently in the DSH and HMenh tests but the LWC in the stratiform region is also reduced, with the stratocumulus cloud layer displaying breaks that are not SCT-related (Figures 4.4d-e). The incorporation of the collisional break-up mechanism (Figures 4.4b-c) improves the simulation of LWC values in the cumulus region, as well as the prediction of the location of the transition, especially in the BR0.4 scenario where the colliding particles are assumed to be heavily rimed. However, the LWC in the stratocumulus region in these simulations is largely underestimated, with most of the values dropping below 0.4 g/m^3 in the BR0.4 case and the cloud layer appearing thinner and more discontinuous. In all cases, the break-up occurs abruptly in contrast to the

gradual dissipation of the stratiform layer and the formation of shallow trade cumuli that are shown by the observational data (Figure 4.4f). Therefore, the transition appears to be attributed to the increased precipitation that is generated by the SIP mechanisms. The simulations do not show any evidence of low-level temperature inversion and boundary layer decoupling (Figure 4.5f). It is clear however that the latent heat released during the additional phase changes caused by the SIP mechanisms led to the warming of the top of the boundary layer, especially in the BR02 and BR0.4 cases where the temperature was increased by almost 2°C (Figures 4.5b-c). The weakening of the temperature inversion at the cloud top and, as a result, the intrusion of free tropospheric air could potentially have contributed to the excessive break-up of both the stratocumulus and cumulus regions.

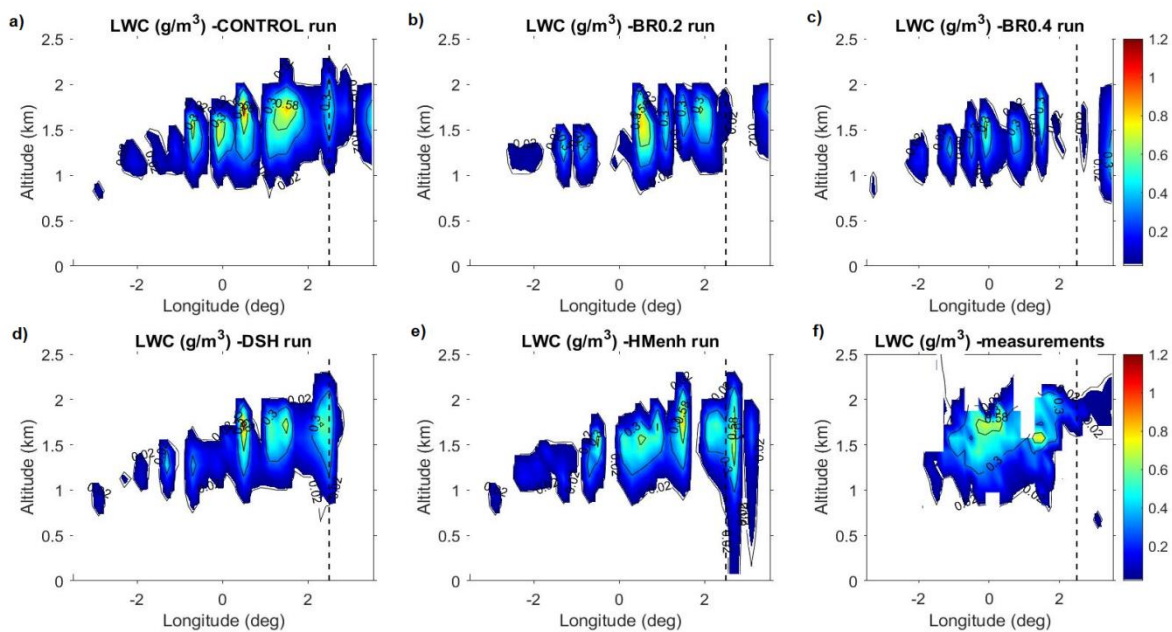


Figure 4.4 Liquid Water Content values plotted along the flight path in each simulation and aircraft measurements (bottom right plot). The 2.5° meridian is denoted with a dashed vertical line and represents the location of the transition.

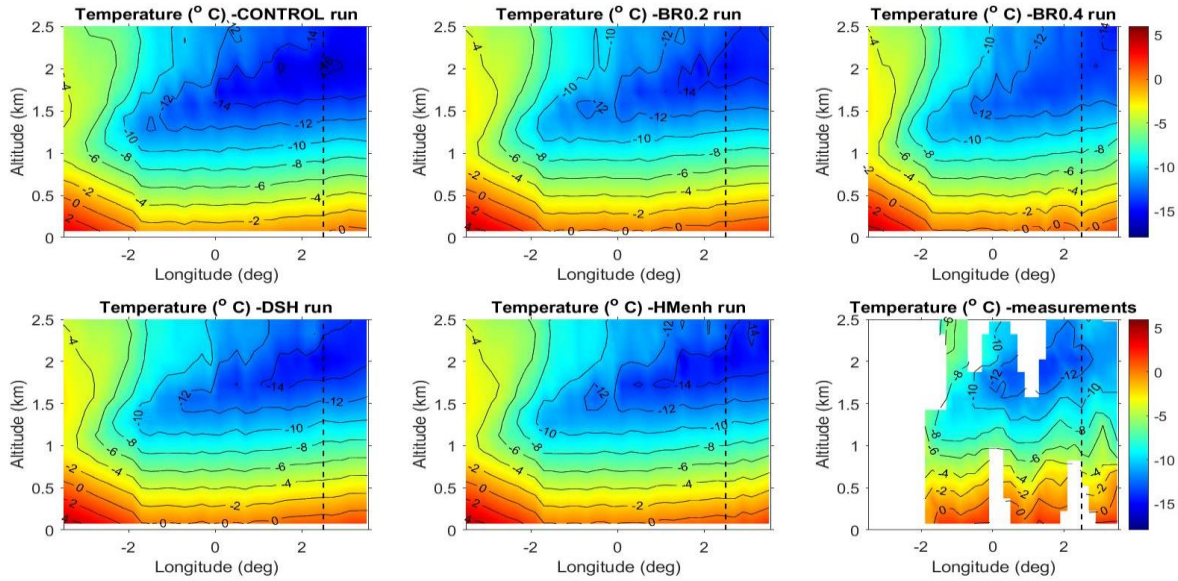


Figure 4.5 Air temperature values plotted along the flight path in each simulation and aircraft measurements (bottom right plot). The 2.5° meridian is denoted with a dashed vertical line and represents the location of the transition.

The number concentration of hydrometeors of effective radius greater than $100\mu\text{m}$ predicted in each simulation as a function of temperature is presented in Figure 4.6, along with the CIP-100 and 2DS probe measurements. For the purpose of the accurate comparison with the observations, modeled values below the probes' threshold (10^{-2} L^{-1}) were not included in the calculation of the averages. In the stratiform region (Figure 4.6a), the number concentration of large particles produced by the CONTROL simulation does not seem to vary significantly with temperature, in accordance with observations, but remains mostly around the 10^{-2} L^{-1} limit, rarely surpassing it. The implementation of the DSH and HMenh mechanisms is not successful at generating additional particles, with concentrations remaining low at all levels within the boundary layer. The BR0.2 and BR0.4 tests show that the collisional break-up process is highly effective in producing new particles, with the results improving by at least one order of magnitude in both cases.

In the cumulus region (Figure 4.6b), the number concentrations in the CONTROL simulation show an increase of almost 0.05 L^{-1} compared to the respective values in the stratiform region, which indicates that the formation of precipitable particles is inadequate and explains the weaker representation of the SCT. The DSH and HMenh values fluctuate around 10^{-1} L^{-1} , therefore causing a slight improvement in the results of the CONTROL simulation with the DSH mechanism appearing to be the most effective of the two. BR0.2 and BR0.4 majorly enhance the simulated values, with the BR0.4 scenario providing the best fit to the observational curve, but tend to overestimate the new particle production at higher temperatures ($>-3^\circ\text{C}$).

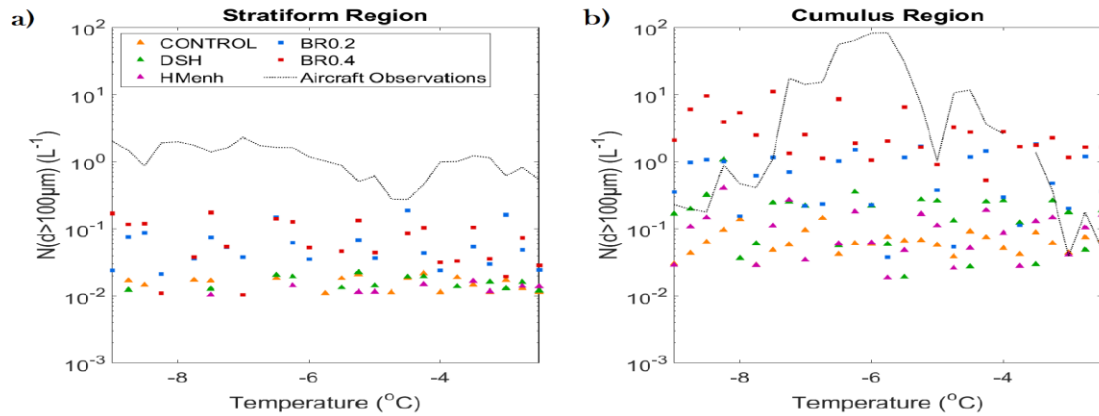


Figure 4.6 Number concentration of particles larger than $100 \mu\text{m}$ as a function of temperature. Data are binned in 0.5°C and lower than 0.01 L^{-1} are excluded for the calculation of the averages.

The frequency of appearance of large particle number concentration values is demonstrated in Figure 4.7. In the stratiform region (Figure 4.7a) the $N(d>100 \mu\text{m})$ values predicted by the CONTROL test reach 10^{-1} L^{-1} , with the vast majority found accumulated near the 10^{-2} L^{-1} threshold. The larger values displayed in the observed frequency distribution ($>10^0 \text{ L}^{-1}$) fail to be reproduced. The DSH and HMenh scenarios demonstrate similar results, with their curves occasionally overlapping. Their predicted maximum values are smaller than 10^{-1} L^{-1} , suggesting that these SIP mechanisms are unable to generate new particles, larger than $100 \mu\text{m}$, in this area. The results from the BR0.2 test show some relative improvement, with number concentration values reaching and surpassing 10^{-1} L^{-1} in rather low frequencies. The BR0.4 test is the most successful in simulating number concentrations with values as high as 1 L^{-1} but the frequency of appearance remains highly underestimated.

In the cumulus region (Figure 4.7b), the CONTROL simulation appears to be underperforming, mainly producing values lower than $5 \times 10^{-2} \text{ L}^{-1}$. HMenh, DSH and BR0.2 visibly improve the results, generating number concentration values up to 2, 5 and 30 L^{-1} . In addition, the DSH and BR0.2 runs predict the frequency of appearance of number concentrations up to 10^0 L^{-1} with relative accuracy. The BR0.4 simulated frequency distribution is the most consistent with the aircraft measurements, while the maximum $N(d>100 \mu\text{m})$ value surpasses 100 L^{-1} . It is evident that the collisional break-up mechanism produces precipitation at a much higher rate, in comparison to the other SIP mechanisms. Furthermore, the assumed rime fraction of the colliding particles also plays a key role in the formation of precipitation-size particles which explains why its application in the WRF simulations is so impactful for the SCT.

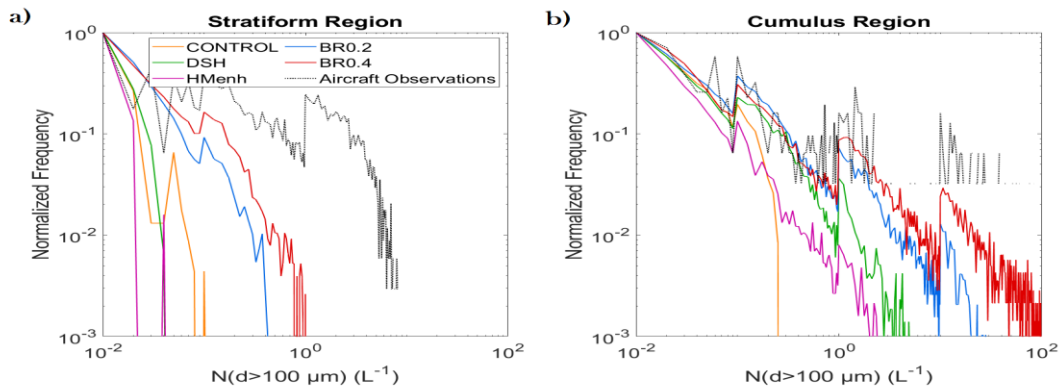


Figure 4.7 Relative frequency distribution of particles larger than 100 μm . Data are binned in intervals ranging from 0.01 L^{-1} for small concentration values to 0.6 L^{-1} for large concentration values and scaled with maximum frequency.

The combined effect of the individual mechanisms is discussed in the following section. In Figures 4.8 and 4.9, the LWP maps at 1200 UTC and LWP time series of ALL0.2 and ALL0.4 are pictured. The simulations bare a significant resemblance to the BR0.2 and BR0.4 sensitivity tests, with the LWC and LWP being underpredicted in the stratiform area, especially in the ALL0.4 case (Figure 4.8b) and the stratocumulus layer displaying discontinuities. This is an indication that the collisional break-up mechanism overpowers the rest of the SIP processes and confirms that the value of the rimed fraction is consequential. The ALL0.4 scenario (Figure 4.9b) accurately predicts the drop in LWP values that suggests the transition of the cloud regime, in contrast to the ALL0.2 scenario (Figure 4.9a), in which the transition appears to be delayed.

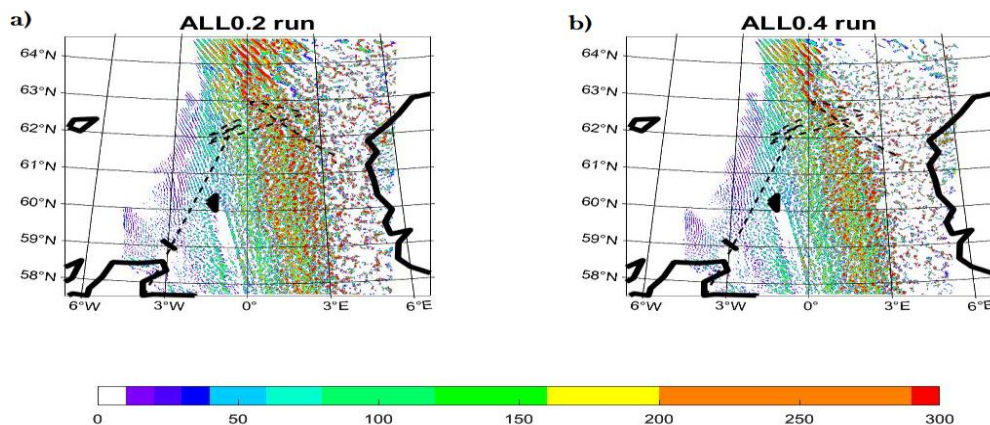


Figure 4.8 Liquid Water Path (LWP) maps of each simulation at 1200 UTC. Values lower than 10 g/m^2 are being ignored in order to enable the depiction of cloud free conditions.

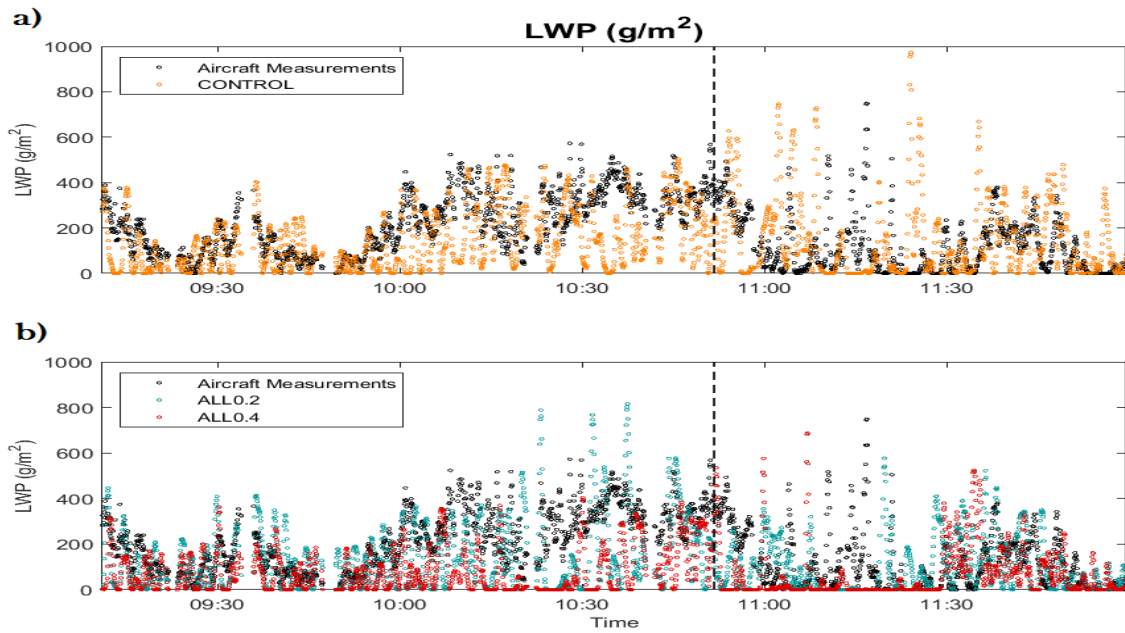


Figure 4.9 Time-series of the simulated LWP values in each scenario and the aircraft measurements along the flight path. The time of the aircraft crosses the cloud transition is denoted with a dashed vertical line.

The number concentration values that are simulated in the ALL0.2 and ALL0.4 cases show a vast improvement when compared to the CONTROL simulation, as shown in Figure 4.10 and 4.11. The excessive production of ice that glaciates the stratocumulus cloud, as suggested by the severe drop in LWP (Figure 4.9b), leads to the generation of large particles in concentrations comparable to the observations in that area. However, in the cumulus region, the simulated curves do not diverge significantly from the respective BR0.2 and BR0.4 tests, which signals that collisional break-up is the main contributor to the formation of precipitation.

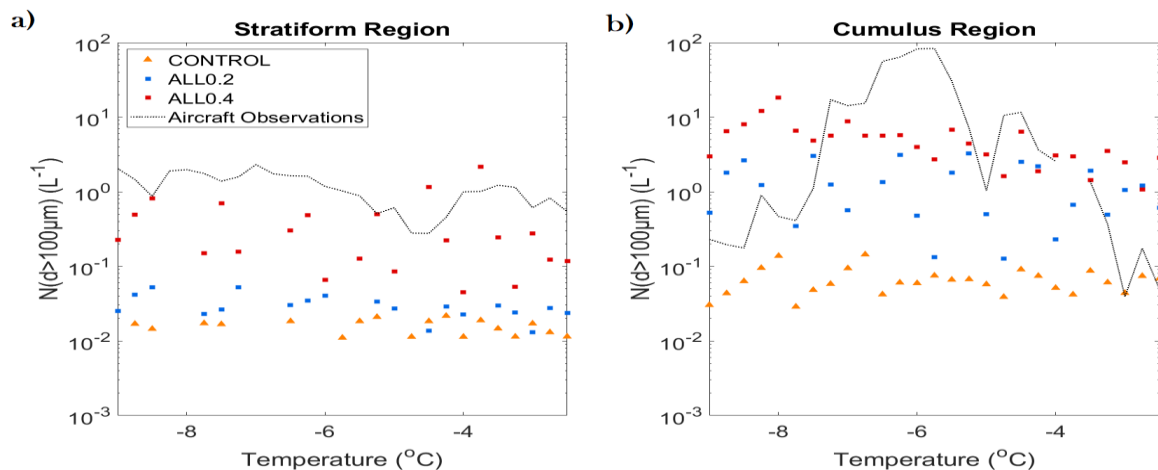


Figure 4.10 Number concentration of particles larger than $100 \mu\text{m}$ as a function of temperature. Data are binned in 0.5°C and lower than 0.01 L^{-1} are excluded for the calculation of the averages.

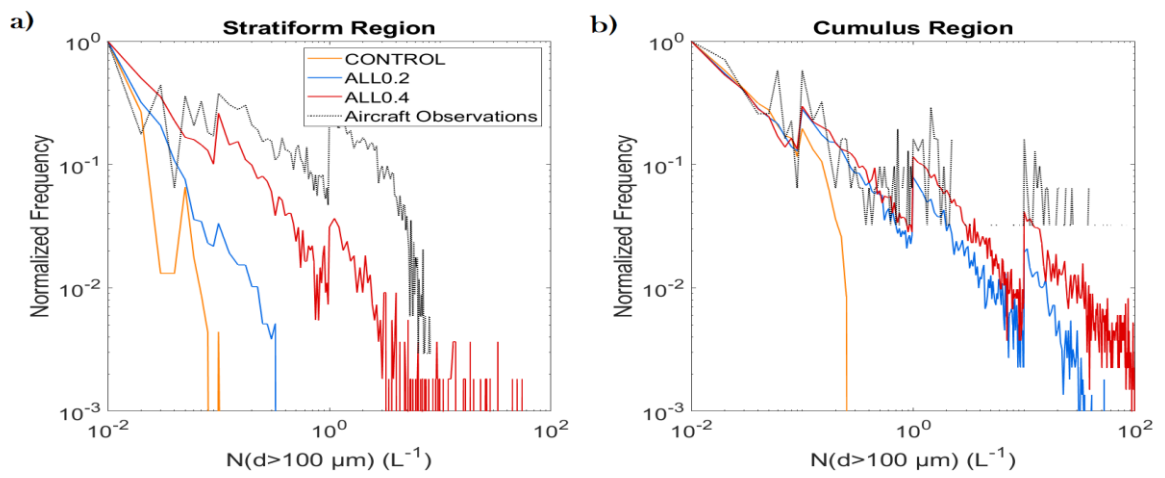


Figure 4.11 Relative frequency distribution of particles larger than 100 μm. Data are binned in intervals ranging from 0.01 L^{-1} for small concentration values to 0.6 L^{-1} for large concentration values and scaled with maximum frequency.

5. Conclusions

This study investigates the effect of secondary ice production mechanisms on the stratocumulus-to-cumulus transition through simulations using the WRF model. In the CONTROL test, the forcing of precipitation by the imposed drop in the number concentration of droplets was successful in triggering the break-up of the stratiform cloud. In this test, the Stratocumulus layer was accurately simulated but the decrease in LWP was largely underpredicted and the transition to the Cumulus regime was delayed. The break-up is more prominently featured in all the SIP simulations due to the production of additional precipitation while the formation of Cu clouds was also well-represented in the convective region. This confirms the importance of precipitation in the initiation of the SCT argued by Abel et al. (2017) and Yamaguchi et al. (2017). However the evaporation-induced temperature inversion that was a key element in these theories was not successfully represented in our simulations.

Collisional break-up is the most effective in the generating participation-sized particles, especially in the Cumulus region, as well as representing the depletion of LWP post-transition, with the predicted values adequately approaching the observations provided by Abel et al. (2017). In addition, the results show a significant dependency of the simulated cloud properties on the assumed value of the rimed-fraction of the colliding particles, with LWP values in the case of more heavily rimed particles (BR0.4) being accurately predicted in the Cumulus region, but severely underestimated in the Stratocumulus region. It is worth noting, however, that BR0.4 is the only case in which the transition was displaced westward, matching its observed location.

The droplet shattering and the enhanced Hallett-Mossop mechanism tests showed little improvement in the prediction of the number concentration of large hydrometeors and LWP of the Cumulus cloud area but maintained a relatively good representation of the Stratocumulus cloud, in contrast with Abel's UNIFIED model simulations in which the supercooled water was overwhelmingly depleted by ice production processes. However, these mechanisms failed to produce large particles in number concentrations comparable to measurements.

The similarities in the results of the collisional break-up and combined SIP effect (ALL0.2 and ALL0.4) tests suggest that the generation of additional precipitable particles and the subsequent draining of the Stratocumulus cloud are predominantly accomplished by the collisional break-up mechanisms. Even though the simulated temperature conditions are favorable for the activation of the Hallett-Mossop effect, this mechanism, even in its enhanced form, severely underperforms and appears to be overpowered by collisional break-up in ALL0.2 and ALL0.4 tests. This is of great importance since the H-M mechanism is widely represented in mesoscale and cloud

resolving models whereas collisional break-up is not typically incorporated in microphysics parameterization schemes.

The treatment of droplet number concentration (through coupling with chemistry) and rime fraction as prognostic variables are proposed for future research in order to test the model's ability to spontaneously activate the SCT and achieve more realistic simulations.

References

Abel, S. J., Boutle, I. A., Waite, K., Fox, S., Brown, P. R. A., Cotton, R., Lloyd, G., Choullarton, T. W., & Bower, K. N. (2017). The Role of Precipitation in Controlling the Transition from Stratocumulus to Cumulus Clouds in a Northern Hemisphere Cold-Air Outbreak, *Journal of the Atmospheric Sciences*, 74(7), 2293-2314. <https://doi.org/10.1175/JAS-D-16-0362.1>

Atkinson, B. W., and Wu Zhang, J. (1996), Mesoscale shallow convection in the atmosphere, *Rev. Geophys.*, 34(4), 403– 431, doi:10.1029/96RG02623.

Atlas, R. L., Bretherton, C. S., Blossey, P. N., Gettelman, A., Bardeen, C., Lin, P., and Ming, Y.: How well do large-eddy simulations and global climate models represent observed boundary layer structures and low clouds over the summertime Southern Ocean?, *J. Adv. Model. Earth Sy.*, 12, e2020MS002205, <https://doi.org/10.1029/2020MS002205>, 2020

Bony, Sandrine, Robert Colman, Vladimir M. Kattsov, Richard P. Allan, Christopher S. Bretherton, Jean-Louis Dufresne, Alex Hall, Stephane Hallegatte, Marika M. Holland, William Ingram, David A. Randall, Brian J. Soden, George Tselioudis, and Mark J. Webb. " How Well Do We Understand and Evaluate Climate Change Feedback Processes?". *Journal of Climate* 19.15 (2006): 3445-3482. <https://doi.org/10.1175/JCLI3819.1>

Bretherton, C. S., &Wyant, M. C. (1997). Moisture Transport, Lower-Tropospheric Stability, and Decoupling of Cloud-Topped Boundary Layers, *Journal of the Atmospheric Sciences*, 54(1), 148-167. [https://doi.org/10.1175/1520-0469\(1997\)054<0148:MTL TSA>2.0.CO;2](https://doi.org/10.1175/1520-0469(1997)054<0148:MTL TSA>2.0.CO;2)

Bullard, J. E., et al. (2016), High-latitude dust in the Earth system, *Rev. Geophys.*, 54, 447– 485, doi:[10.1002/2016RG000518](https://doi.org/10.1002/2016RG000518).

C.P.R Saunders, A.S Hosseini, A laboratory study of the effect of velocity on Hallett–Mossop ice crystal multiplication, *Atmospheric Research*, Volumes 59–60, 2001, Pages 3-14, ISSN 0169-8095, [https://doi.org/10.1016/S0169-8095\(01\)00106-5](https://doi.org/10.1016/S0169-8095(01)00106-5).

Chen, T., Rossow, W. B., and Zhang, Y. (2000). Radiative Effects of Cloud-Type Variations. *Journal of Climate* 13, 1, 264-286, available from: <[https://doi.org/10.1175/1520-0442\(2000\)013<0264:REOCTV>2.0.CO;2](https://doi.org/10.1175/1520-0442(2000)013<0264:REOCTV>2.0.CO;2)>

Choullarton, T.W., Griggs, D.J., Humood, B.Y. and Latham, J. (1980), Laboratory studies of riming, and its relation to ice splinter production. *Q.J.R. Meteorol. Soc.*, 106: 367-374. <https://doi.org/10.1002/qj.49710644809>

Chung, D., G. Matheou, and J. Teixeira. " Steady-State Large-Eddy Simulations to Study the Stratocumulus to Shallow Cumulus Cloud Transition". *Journal of the Atmospheric Sciences* 69.11 (2012): 3264-3276. <<https://doi.org/10.1175/JAS-D-11-0256.1>>. Web. 21 Mar. 2021.

Clark, P., Choullarton, T. W., Brown, P. R. A., Field, P. R., Illingworth, A. J., and Hogan, R. J.: Numerical modeling of mixed-phase frontal clouds observed during the CWVC project, *Q. J. Roy. Meteor. Soc.*, 131, 1677 1693, <https://doi.org/10.1256/qj.03.210>, 2005

Conen, F., Stopelli, E., and Zimmermann, L.: Clues that decaying leaves enrich Arctic air with ice nucleating particles, *Atmos. Environ.*, 129, 91–94, <https://doi.org/10.1016/j.atmosenv.2016.01.027>, 2016.

Connolly, P.J., Heymsfield, A.J. and Choullarton, T.W. (2006), Modelling the influence of rimer surface temperature on the glaciation of intense thunderstorms: The rime–splinter mechanism of ice multiplication. *Q.J.R. Meteorol. Soc.*, 132: 3059-3077. <https://doi.org/10.1256/qj.05.45>

Creamean, J. M., Cross, J. N., Pickart, R., McRaven, L., Lin, P., Pacini, A., Hanlon, R., Schmale, D. G., Ceniceros, J., Aydell, T., Colombi, N., Bolger, E., and DeMott, P. J.: Ice Nucleating Particles Carried From Below a Phytoplankton Bloom to the Arctic Atmosphere, *Geophys. Res. Lett.*, 46, 8572–8581, <https://doi.org/10.1029/2019GL083039>, 2019.

D. Baumgardner, J.L. Brenguier, A. Bucholtz, H. Coe, P. DeMott, T.J. Garrett, J.F. Gayet, M. Hermann, A. Heymsfield, A. Korolev, M. Krämer, A. Petzold, W. Strapp, P. Pilewskie, J. Taylor, C. Twohy, M. Wendisch, W. Bachalo, P. Chuang, Airborne instruments to measure atmospheric aerosol particles, clouds and radiation: A cook's tour of mature and emerging technology, *Atmospheric Research*, Volume 102, Issues 1–2, 2011, Pages 10-29, ISSN 0169-8095, <https://doi.org/10.1016/j.atmosres.2011.06.021>.

de Roode, S. R., & Duynkerke, P. G. (1997). Observed Lagrangian Transition of Stratocumulus into Cumulus during ASTEX: Mean State and Turbulence Structure, *Journal of the Atmospheric Sciences*, 54(17), 2157-2173. [https://doi.org/10.1175/1520-0469\(1997\)054<2157:OLTOSI>2.0.CO](https://doi.org/10.1175/1520-0469(1997)054<2157:OLTOSI>2.0.CO);

Dearden, C., Vaughan, G., Tsai, T., and Chen, J.: Exploring the diabatic role of ice microphysical processes in two North Atlantic summer cyclones, *Mon. Weather Rev.*, 144, 1249–1272, <https://doi.org/10.1175/MWR-D-15-0253.1>, 2016.

DeMott, P. J., Hill, T. C. J., McCluskey, C. S., Prather, K. A., Collins, D. B., Sullivan, R. C., Ruppel, M. J., Mason, R. H., Irish, V. E., Lee, T., Hwang, C. Y., Rhee, T. S., Snider, J. R., McMeeking, G. R., Dhaniyala, S., Lewis, E. R., Wentzell, J. J. B., Abbatt, J., Lee, C., Sultana, C. M., Ault, A. P., Axson, J. L., Diaz Martinez, M., Venero, I., Santos-Figueroa, G., Stokes, M. D., Deane, G. B., Mayol-Bracero, O. L., Grassian, V. H., Bertram, T. H., Bertram, A. K., Moffett, B. F., and Franc, G. D.: Sea spray aerosol as a unique source of ice nucleating particles, *P. Natl. Acad. Sci. USA*, 113, 5797–5803, <https://doi.org/10.1073/pnas.1514034112>, 2016.

Dong, Y.Y. and Hallett, J. (1989), Droplet accretion during rime growth and the formation of secondary ice crystals. *Q.J.R. Meteorol. Soc.*, 115: 127-142. <https://doi.org/10.1002/qj.49711548507>

Dudhia, J., 1989: Numerical study of convection observed during the Winter Monsoon Experiment using a mesoscale two-dimensional model. *J. Atmos. Sci.*, 46, 3077–3107.
E.M. Agee, Mesoscale cellular convection over the oceans, *Dynamics of Atmospheres and Oceans*, Volume 10, Issue 4, 1987, Pages 317-341, ISSN 0377-0265, [https://doi.org/10.1016/0377-0265\(87\)90023-6](https://doi.org/10.1016/0377-0265(87)90023-6).

Feingold, G., B. Stevens, W. R. Cotton, and R. L. Walko, 1994: An explicit cloud microphysical/LES model designed to simulate the Twomey effect. *Atmos. Res.*, 33, 207–233.

Feingold, G., Koren, I., Yamaguchi, T., and Kazil, J.: On the reversibility of transitions between closed and open cellular convection, *Atmos. Chem. Phys.*, 15, 7351–7367, <https://doi.org/10.5194/acp-15-7351-2015>, 2015.

Ferrier, B. S., 1994: A double-moment multiple-phase four-class bulk ice scheme. Part I: Description. *J. Atmos. Sci.*, 51, 249-280.

Field, P. R., R. P. Lawson, P. R. A. Brown, G. Lloyd, C. Westbrook, D. Moisseev, A. Miltenberger, A. Nenes, A. Blyth, T. Choulaton, P. Connolly, J. Buehl, J. Crosier, Z. Cui, C. Dearden, P. DeMott, A. Flossmann, A. Heymsfield, Y. Huang, H. Kalesse, Z. A. Kanji, A. Korolev, A. Kirchgaessner, S. Lasher-Trapp, T. Leisner, G. McFarquhar, V. Phillips, J. Stith, and S. Sullivan. " Secondary Ice Production: Current State of the Science and Recommendations for the Future". *Meteorological Monographs* 58 (2017): 7.1-7.20. < <https://doi.org/10.1175/AMSMONOGRAPHS-D-16-0014.1>>.

Fletcher, Jennifer, Shannon Mason, and Christian Jakob. " The Climatology, Meteorology, and Boundary Layer Structure of Marine Cold Air Outbreaks in Both Hemispheres". *Journal of Climate* 29.6 (2016): 1999-2014. < <https://doi.org/10.1175/JCLI-D-15-0268.1>>. Web. 21 Mar. 2021.

- Fowler, L. D., D. A. Randall, and S. A. Rutledge, 1996: Liquid and ice microphysics in the CSU General Circulation Model. Part 1: Model description and simulated microphysical processes. *J. Climate*, 9, 489–529.
- Fridlind, A. M., Ackerman, A. S., McFarquhar, G., Zhang, G., Poellot, M. R., DeMott, P. J., Prenni, A. J., and Heymsfield, A. J. (2007), Ice properties of single-layer stratocumulus during the Mixed-Phase Arctic Cloud Experiment: 2. Model results, *J. Geophys. Res.*, 112, D24202, doi:[10.1029/2007JD008646](https://doi.org/10.1029/2007JD008646).
- Glassmeier, F. and Lohmann, U.: Constraining precipitation with susceptibility of warm-, ice-, and mixed-phase clouds with microphysical equations, *J. Atmos. Sci.*, 73, 5003–5023, <https://doi.org/10.1175/JAS-D-16-0008.1>, 2016.
- Griggs, D.J. and Choullarton, T.W. (1983), Freezing modes of riming droplets with application to ice splinter production. *Q.J.R. Meteorol. Soc.*, 109: 243-253. <https://doi.org/10.1002/qj.49710945912>
- HALLETT, J., MOSSOP, S. Production of secondary ice particles during the riming process. *Nature* 249, 26–28 (1974). <https://doi.org/10.1038/249026a0>
- Harrington, T. Reisen, W. R. Cotton, and S. M. Kreidenweis, 1999: Cloud resolving simulations of Arctic stratus. Part II: Transition-season clouds. *Atmos. Res.*, 51, 45–75.
- Heymsfield, A.J. and Mossop, S.C. (1984), Temperature dependence of secondary ice crystal production during soft hail growth by riming. *Q.J.R. Meteorol. Soc.*, 110: 765-770. <https://doi.org/10.1002/qj.49711046512>
- Hobbs, Peter V., and Arthur L. Rangno. " Ice Particle Concentrations in Clouds". *Journal of Atmospheric Sciences* 42.23 (1985): 2523-2549. <[https://doi.org/10.1175/1520-0469\(1985\)042<2523:IPCIC>2.0.CO;2](https://doi.org/10.1175/1520-0469(1985)042<2523:IPCIC>2.0.CO;2)>.
- Irish, V. E., Elizondo, P., Chen, J., Chou, C., Charette, J., Lizotte, M., Ladino, L. A., Wilson, T. W., Gosselin, M., Murray, B. J., Polishchuk, E., Abbatt, J. P. D., Miller, L. A., and Bertram, A. K.: Ice-nucleating particles in Canadian Arctic sea-surface microlayer and bulk seawater, *Atmos. Chem. Phys.*, 17, 10583–10595, <https://doi.org/10.5194/acp-17-10583-2017>, 2017
- Irish, V. E., Hanna, S. J., Xi, Y., Boyer, M., Polishchuk, E., Ahmed, M., Chen, J., Abbatt, J. P. D., Gosselin, M., Chang, R., Miller, L. A., and Bertram, A. K.: Revisiting properties and concentrations of ice-nucleating particles in the sea surface microlayer and bulk seawater in the Canadian Arctic during summer, *Atmos. Chem. Phys.*, 19, 7775–7787, <https://doi.org/10.5194/acp19-7775-2019>, 2019
- Jiang, H., G. Feingold, W. R. Cotton, and P. G. Duynkerke, 2001: Large-eddy simulation of entrainment of cloud condensation nuclei into the arctic boundary layer: May 18, 1998 FIRE/ SHEBA case study. *J. Geophys. Res.*, 106, 15 113–15 122.
- Kenneth V. Beard, Ice initiation in warm-base convective clouds: An assessment of microphysical mechanisms, *Atmospheric Research*, Volume 28, Issue 2, 1992, Pages 125-152, ISSN 0169-8095, [https://doi.org/10.1016/0169-8095\(92\)90024-5](https://doi.org/10.1016/0169-8095(92)90024-5).
- Khvorostyanov, V. I., 1995: Mesoscale processes of cloud formation, cloud-radiation and their modeling with explicit microphysics. *Atmos. Res.*, 39, 1–67.
- Kidston, J., Scaife, A., Hardiman, S. et al. Stratospheric influence on tropospheric jet streams, storm tracks and surface weather. *Nature Geosci* 8, 433–440 (2015). <https://doi.org/10.1038/ngeo2424>
- Kolstad, E.W., Bracegirdle, T.J. Marine cold-air outbreaks in the future: an assessment of IPCC AR4 model results for the Northern Hemisphere. *ClimDyn* 30, 871–885 (2007).<https://doi.org/10.1007/s00382-007-0331-0>

Kolstad, E.W., Breiteig, T. and Scaife, A.A. (2010), The association between stratospheric weak polar vortex events and cold air outbreaks in the Northern Hemisphere. *Q.J.R. Meteorol. Soc.*, 136: 886-893. <https://doi.org/10.1002/qj.620>

Kolstad, E. W., , T. J. Bracegirdle, , and I. A. Seierstad, 2009: Marine cold-air outbreaks in the North Atlantic: Temporal distribution and associations with large-scale atmospheric circulation. *Climate Dyn.*, 33, 187–197, doi:10.1007/s00382-008-0431-5

Korolev, A. V., J. W. Strapp, G. A. Isaac, and A. N. Nevzorov. " The Nevzorov Airborne Hot-Wire LWC–TWC Probe: Principle of Operation and Performance Characteristics". *Journal of Atmospheric and Oceanic Technology* 15.6 (1998): 1495-1510. <[https://doi.org/10.1175/1520-0426\(1998\)015<1495:TNAHWL>2.0.CO;2](https://doi.org/10.1175/1520-0426(1998)015<1495:TNAHWL>2.0.CO;2)>.

Krueger, S. K., McLean, G. T., & Fu, Q. (1995). Numerical Simulation of the Stratus-to-Cumulus Transition in the Subtropical Marine Boundary Layer. Part I: Boundary-Layer Structure, *Journal of Atmospheric Sciences*, 52(16), 2839-2850. [https://doi.org/10.1175/1520-0469\(1995\)052<2839:NSOTST>2.0.CO;2](https://doi.org/10.1175/1520-0469(1995)052<2839:NSOTST>2.0.CO;2)

Lau, K.-M. and Wu, H.-T.: Climatology and changes in tropical ocean rainfall characteristics inferred from Tropical Rainfall Measuring Mission (TRMM) data (1998–2009), *J. Geophys. Res.*, 116, D17111, <https://doi.org/10.1029/2011JD015827>, 2011.

Lewellen, D. C., Lewellen, W. S., & Yoh, S. (1996). Influence of Bowen Ratio on Boundary-Layer Cloud Structure, *Journal of Atmospheric Sciences*, 53(1), 175-187. [https://doi.org/10.1175/1520-0469\(1996\)053<0175:IOBROB>2.0.CO;2](https://doi.org/10.1175/1520-0469(1996)053<0175:IOBROB>2.0.CO;2)

Lin, Y.-L., R. D. Farley, and H. D. Orville, 1983: Bulk parameterization of the snow field in a cloud model. *J. Climate Appl.*

Mason and J. Maybank, 1960: The fragmentation and electrification of freezing water drops. *Quart. J. Roy. Meteor. Soc.*, 86, 176–185, doi:10.1002/qj.49708636806

Mason, B.J. (1996), The rapid glaciation of slightly supercooled cumulus clouds. *Q.J.R. Meteorol. Soc.*, 122: 357-365. <https://doi.org/10.1002/qj.49712253003>

McGrath, Andrew, and Tim Hewison. " Measuring the Accuracy of MARSS—An Airborne Microwave Radiometer". *Journal of Atmospheric and Oceanic Technology* 18.12 (2001): 2003-2012. [https://doi.org/10.1175/1520-0426\(2001\)018<2003:MTAOMA>2.0.CO;2](https://doi.org/10.1175/1520-0426(2001)018<2003:MTAOMA>2.0.CO;2).

Meyers, M. P., R. L. Walko, J. Y. Harrington, and W. R. Cotton, 1997: New RAMS cloud microphysics parameterization. Part II: The two-moment scheme. *Atmos. Res.*, 45, 3–39.

Morrison, H., J. A. Curry, and V. I. Khvorostyanov. " A New Double-Moment Microphysics Parameterization for Application in Cloud and Climate Models. Part I: Description". *Journal of the Atmospheric Sciences* 62.6 (2005): 1665-1677. <<https://doi.org/10.1175/JAS3446.1>>.

Mossop, S.C. (1985), Secondary ice particle production during rime growth: The effect of drop size distribution and rimer velocity. *Q.J.R. Meteorol. Soc.*, 111: 1113-1124. <https://doi.org/10.1002/qj.4971114701>

Mossop, S.C., Brownscombe, J.L. and Collins, G.J. (1974), The production of secondary ice particles during riming. *Q.J.R. Meteorol. Soc.*, 100: 427-436. <https://doi.org/10.1002/qj.49710042514>

Murray, B. J., Carslaw, K. S., and Field, P. R.: Opinion: Cloud-phase climate feedback and the importance of ice-nucleating particles, *Atmos. Chem. Phys.*, 21, 665–679, <https://doi.org/10.5194/acp-21-665-2021>, 2021.

National Weather Service, National Oceanic And Atmospheric Administration, <https://www.weather.gov/>

Papritz, L., S. Pfahl, H. Sodemann, and H. Wernli, 2015: A climatology of cold air outbreaks and their impact on air–sea heat fluxes in the high-latitude South Pacific. *J. Climate*, 28, 342–364, doi:10.1175/JCLI-D-14-00482.1.

Phillips, V. T. J., Patade, S., Gutierrez, J., and Bansemer, A.: Secondary ice production by fragmentation of freezing drops: Formulation and theory, *Journal of the Atmospheric Sciences*, 75, 3031–3070, 10.1175/JAS-D-17-0190.1, 2018.

Phillips, V. T. J., J. Yano, and A. Khain, 2017: Ice multiplication by breakup in ice–ice collisions. Part I: Theoretical formulation. *J. Atmos. Sci.*, 74, 1705–1719, doi:10.1175/JAS-D-16-0224.1.

Prospero, J. M., Bullard, J. E., and Hodgkins, R.: High-Latitude Dust Over the North Atlantic: Inputs from Icelandic Proglacial Dust Storms, *Science*, 335, 1078–1082, 2012

Reisner, J., R. M. Rasmussen, and R. T. Bruintjes, 1998: Explicit forecasting of supercooled liquid water in winter storms using the MM5 forecast model. *Quart. J. Roy. Meteor. Soc.*, 124, 1071–1107.

Ren, R-C., and Ming Cai. " Meridional and Downward Propagation of Atmospheric Circulation Anomalies. Part II: Southern Hemisphere Cold Season Variability". *Journal of the Atmospheric Sciences* 65.7 (2008): 2343-2359. <<https://doi.org/10.1175/2007JAS2594.1>>.

Rogers, J. C., & Rohli, R. V. (1991). Florida Citrus Freezes and Polar Anticyclones in the Great Plains, *Journal of Climate*, 4(11), 1103–1113. [https://doi.org/10.1175/1520-0442\(1991\)004<1103:FCFAPA>2.0.CO;2](https://doi.org/10.1175/1520-0442(1991)004<1103:FCFAPA>2.0.CO;2)

S. Matsumoto, M. Iida, M. Takeuchi, T. Asai and K. Ninomiya (1963), A Note on the Mechanism of Cold Air Outbreak

Sanchez-Marroquin, A., Arnalds, O., Baustian-Dorsi, K. J., Browse, J., Dagsson-Waldhauserova, P., Harrison, A. D., Maters, E. C., Pringle, K. J., Vergara-Temprado, J., Burke, I. T., McQuaid, J. B., Carslaw, K. S., and Murray, B. J.: Iceland is an episodic source of atmospheric ice-nucleating particles relevant for mixed-phase clouds, *Sci. Adv.*, 6, eaba8137, <https://doi.org/10.1126/sciadv.aba8137>, 2020.

Sandu, Irina, and Bjorn Stevens. " On the Factors Modulating the Stratocumulus to Cumulus Transitions". *Journal of the Atmospheric Sciences* 68.9 (2011): 1865-1881. <<https://doi.org/10.1175/2011JAS3614.1>>.

Scaife AA, Folland CK, Alexander LV, Moberg A, Knight JR. 2008. European climate extremes and the North Atlantic Oscillation. *J. Climate* 21: 72–83.

Schnell, R. C. and Vali, G.: Freezing nuclei in marine waters, *Tellus*, 27, 321–323, <https://doi.org/10.3402/tellusa.v27i3.9911>, 1975.

Schnell, R. C. and Vali, G.: Biogenic ice nuclei .1. terrestrial and marine sources, *J. Atmos. Sci.*, 33, 1554–1564, [https://doi.org/10.1175/1520-0469\(1976\)0332.0.co;2](https://doi.org/10.1175/1520-0469(1976)0332.0.co;2), 1976.

Schnell, R. C.: Ice Nuclei in Seawater, Fog Water and Marine Air off the Coast of Nova Scotia: Summer 1975, *J. Atmos. Sci.*, 34, 1299–1305, [https://doi.org/10.1175/1520-0469\(1977\)034<1299:inisfw>2.0.co;2](https://doi.org/10.1175/1520-0469(1977)034<1299:inisfw>2.0.co;2), 1977.

Slingo, A. and Schrecker, H.M. (1982), On the shortwave radiative properties of stratiform water clouds. *Q.J.R. Meteorol. Soc.*, 108: 407–426. <https://doi.org/10.1002/qj.49710845607>

Smith, E. T., & Sheridan, S. C. (2018). The characteristics of extreme cold events and cold air outbreaks in the eastern United States. *International Journal of Climatology*, 38(S1), e807–e820, <https://doi.org/10.1002/joc.5408>

Smith, E. T., & Sheridan, S. C. (2020). Where do cold air outbreaks occur, and how have they changed over time? *Geophysical Research Letters*, 47, e2020GL086983. <https://doi.org/10.1029/2020GL086983>

Soden, B. J., and Vecchi, G. A. (2011), The vertical distribution of cloud feedback in coupled ocean-atmosphere models, *Geophys. Res. Lett.*, 38, L12704, doi:[10.1029/2011GL047632](https://doi.org/10.1029/2011GL047632).

Sullivan, S. C., Barthlott, C., Crosier, J., Zhukov, I., Nenes, A., and Hoose, C.: The effect of secondary ice production parameterization on the simulation of a cold frontal rainband, *Atmos. Chem. Phys.*, 18, 16461–16480, <https://doi.org/10.5194/acp-18-16461-2018>, 2018.

Taylor, J. W., Choulaton, T. W., Blyth, A. M., Liu, Z., Bower, K. N., Crosier, J., Gallagher, M. W., Williams, P. I., Dorsey, J. R., Flynn, M. J., Bennett, L. J., Huang, Y., French, J., Korolev, A., and Brown, P. R. A.: Observations of cloud microphysics and ice formation during COPE, *Atmos. Chem. Phys.*, 16, 799–826, <https://doi.org/10.5194/acp-16-799-2016>, 2016.

Taylor, P.C. The Role of Clouds: An Introduction and Rapporteur Report. *SurvGeophys* 33, 609–617 (2012). <https://doi.org/10.1007/s10712-012-9182-2>

Thompson, David W. J., Mark P. Baldwin, and John M. Wallace. " Stratospheric Connection to Northern Hemisphere Wintertime Weather: Implications for Prediction". *Journal of Climate* 15.12 (2002): 1421-1428. <[https://doi.org/10.1175/1520-0442\(2002\)015<1421:SCTNHW>2.0.CO;2](https://doi.org/10.1175/1520-0442(2002)015<1421:SCTNHW>2.0.CO;2)>.

Tobo, Y., Adachi, K., DeMott, P. J., Hill, T. C. J., Hamilton, D. S., Mahowald, N. M., Nagatsuka, N., Ohata, S., Uetake, J., Kondo, Y., and Koike, M.: Glacially sourced dust as a potentially significant source of ice nucleating particles, *Nat. Geosci.*, 12, 253–258, <https://doi.org/10.1038/s41561-019-0314-x>, 2019.

van der Dussen, J. J., de Roode, S. R., and Siebesma, A. P.: How large-scale subsidence affects stratocumulus transitions, *Atmos. Chem. Phys.*, 16, 691–701, <https://doi.org/10.5194/acp-16-691-2016>, 2016.

Vardiman, L.: The Generation of Secondary Ice Particles in Clouds by Crystal–Crystal Collision, *J. Atmos. Sci.*, 35, 2168–2180, [https://doi.org/10.1175/1520-0469\(1978\)035<2168:TGOSIP>2.0.CO;2](https://doi.org/10.1175/1520-0469(1978)035<2168:TGOSIP>2.0.CO;2), 1978.

Vavrus, S., Walsh, J.E., Chapman, W.L. and Portis, D. (2006), The behavior of extreme cold air outbreaks under greenhouse warming. *Int. J. Climatol.*, 26: 1133-1147. <https://doi.org/10.1002/joc.1301>

Visagie, P. (1969). Pressures Inside Freezing Water Drops. *Journal of Glaciology*, 8(53), 301-309. doi:10.3189/S0022143000031270

Walko, R., W. R. Cotton, M. P. Meyers, and J. Y. Harrington, 1995: New RAMS cloud microphysics parameterization. Part I: The single-moment scheme. *Atmos. Res.*, 38, 29–62.

Wallace, J. and Hobbs, P. (2006) *Atmospheric Science, Second Edition: An Introductory Survey*, Academic Press.

Walsh, J. E., Phillips, A. S., Portis, D. H., & Chapman, W. L. (2001). Extreme Cold Outbreaks in the United States and Europe, 1948–99, *Journal of Climate*, 14(12), 2642-2658.

Wheeler, D. D., Harvey, V. L., Atkinson, D. E., Collins, R. L., and Mills, M. J. (2011), A climatology of cold air outbreaks over North America: WACCM and ERA-40 comparison and analysis, *J. Geophys. Res.*, 116, D12107, doi:10.1029/2011JD015711.

Wilson, T. W., Ladino, L. A., Alpert, P. A., Breckels, M. N., Brooks, I. M., Browse, J., Burrows, S. M., Carslaw, K. S., Huffman, J. A., Judd, C., Kilhau, W. P., Mason, R. H., McFiggans, G., Miller, L. A., Najera, J. J., Polishchuk, E., Rae, S., Schiller, C. L., Si, M., Temprado, J. V., Whale, T. F., Wong, J. P. S., Wurl, O., Yakobi-Hancock, J. D., Abbatt, J. P. D., Aller, J. Y., Bertram, A. K., Knopf, D. A., and Murray, B. J.: A marine biogenic source of atmospheric ice-nucleating particles, *Nature*, 525, 234–238, <https://doi.org/10.1038/nature14986>, 2015.

Wyant, Matthew C., Christopher S. Bretherton, Hugh A. Rand, and David E. Stevens. " Numerical Simulations and a Conceptual Model of the Stratocumulus to Trade Cumulus Transition". *Journal of the Atmospheric Sciences* 54.1 (1997): 168-192. <[https://doi.org/10.1175/1520-0469\(1997\)054<0168:NSAACM>2.0.CO;2](https://doi.org/10.1175/1520-0469(1997)054<0168:NSAACM>2.0.CO;2)>.

Xiao, H., Wu, CM. & Mechoso, C.R. Buoyancy reversal, decoupling and the transition from stratocumulus to shallow cumulus topped marine boundary layers. *ClimDyn* 37, 971–984 (2011). <https://doi.org/10.1007/s00382-010-0882-3>

Xiao, H., Wu, CM., Mechoso, C.R. et al. A treatment for the stratocumulus-to-cumulus transition in GCMs. *ClimDyn* 39, 3075–3089 (2012). <https://doi.org/10.1007/s00382-012-1342-z>

Yamaguchi, T., Feingold, G., & Kazil, J. (2017). Stratocumulus to cumulus transition by drizzle. *Journal of Advances in Modeling Earth Systems*, 9, 2333–2349, <https://doi.org/10.1002/2017MS001104>

Young, G., Connolly, P. J., Dearden, C., and Choulaton, T. W.: Relating large-scale subsidence to convection development in Arctic mixed-phase marine stratocumulus, *Atmos. Chem. Phys.*, 18, 1475–1494, <https://doi.org/10.5194/acp-18-1475-2018>, 2018.

Young, Kenneth C. " The Role of Contact Nucleation in Ice Phase Initiation in Clouds". *Journal of Atmospheric Sciences* 31.3 (1974): 768-776. <[https://doi.org/10.1175/1520-0469\(1974\)031<0768:TROCNI>2.0.CO;2](https://doi.org/10.1175/1520-0469(1974)031<0768:TROCNI>2.0.CO;2)>.